On information to establish preference between isotropic and transversely isotropic inner core models

Luke Mifflen-Mitchell

A thesis submitted to the
School of Graduate Studies
in partial fulfillment of the
requirements for the degree of
Master of Science

Department of Earth Sciences
Faculty of Science
Memorial University of Newfoundland
St John's, Newfoundland

August, 2015

Abstract

Forward modelling of traveltimes from an inner core model with elliptical velocity dependence was performed, followed by inverse modelling based on both isotropic and elliptically anisotropic (transverse isotropic) traveltimes. The Kolmogorov-Smirnov (KS) test and Bayesian Information Criterion (BIC) were used for establishing model preference.

BIC is a more robust method for studying anisotropy. If we start with an anisotropic model and a large variance of error ($\pm 4\%$), with enough sampling of the anisotropy, even in the case of relatively few traveltime measurements BIC is able to choose correctly the more complicated model as the preferred source model.

It was determined that the KS test is unsuitable for studying inner core anisotropy, but may be useful for studying anisotropy in exploration geophysical methods such as vertical seismic profiling.

Acknowledgements

I would like to acknowledge Dr. Michael Slawinski for his supervision. His thoughtful guidance, resourcefulness and availability for discussions were instrumental in successful completion of this thesis.

Additionally, I would like to acknowledge Dr. Tomasz Danek for his insight into computational methods considered for this thesis.

Lastly, I would like to thank Dr. Mikhail Kotchetov, Nikki Mifflen-Mitchell, David Dalton, and Leia Mifflen-Morrissey for careful proofreading.

Contents

List of Tables

List of Figures

List of Symbols

σ	Stress Tensor*
c, C	Elasticity Tensor
ε	Strain Tensor
v	Wave Velocity
ρ	Density
V	Ray Velocity
qP	Quasi Pressure Wave
Δ	Discriminant
$\boldsymbol{n}$	Normal Vector
ϑ	Wavefront Angle
θ	Ray Angle
V_z	Vertical Ray Velocity
V_x	Horizontal Ray Velocity
t	Traveltime
D	Distance
σ	Standard Deviation*
P	Probability
Φ	Standard Normal Distribution Function
μ	Average Value

L	Likelihood Function
Q	Quality Factor

*Some symbols are used repeatedly with different meanings. In each section the meaning of any repeated symbol is clear.

List of Abbreviations

PREM	Preliminary Reference Earth Model
KS	Kolmogorov-Smirnov
BIC	Bayesian Information Criterion
AIC	Akaike Information Criterion

Chapter 1

Introduction and Historical Background

1.1 Introduction

It is commonly thought in the geophysical community that the inner core of the Earth is anisotropic [11,21]. However, measurements of body waves and the Earth's normal modes can be affected by many different regions as the waves travel through the Earth, making it difficult to reliably determine if, in fact, the inner core is anisotropic. The problem to be addressed is twofold; firstly, if the inner core is indeed anisotropic, can it be determined, and secondly—if so—to quantify the accuracy of measurement needed to determine anisotropy. More specifically, the purpose is to quantify the criteria necessary to give a preference to either an isotropic or transversely isotropic model.

This problem was approached in two steps: a forward problem, and an inverse problem. The forward problem was addressed by creating an approximate model of average properties of the inner core based on the Preliminary Reference Earth Model (PREM) created by Dziewoński and Anderson in 1981 [9]. An elliptical velocity function was used to approximate transversely isotropic inner core velocities.

Traveltime calculations complete the forward model. The inverse model calculates velocity and traveltime values from the forward model traveltimes. Two statistical tests, the Kolmogorov-Smirnov (KS) test, and Bayesian Information Criterion (BIC) were used to assess if there is sufficient information to accept a transversely isotropic model as the cause of variation in measurements.

1.2 Discovery of the Earth's core

There have been many theories throughout history regarding the structure of the Earth; this section is an overview of the scientific research described in the article *Discovery of the Earth's core* by Stephen Brush [5]. Earth's core theories have included speculation of the presence of a completely solid, liquid, or gaseous core. The concept that the Earth has a liquid outer core within a solid shell, and a solid inner core can be traced as far back as the 17th century to Edmund Halley's paper *An Account of the Cause of the Change of the Variation of the Magnetical Needle; With an Hypothesis of the Structure of the Internal parts of the Earth: as it was proposed to the Royal Society in one of their late Meetings* [10]. Halley theorized a magnetic inner core and outer shell to explain variations in magnetic needle observations. However, the scientific community was quite divided about the structure of the Earth until the 20th century. Therefore, it can be said that neither the outer core nor the inner core were discovered prior to the 20th century.

In the late 19th and early 20th century, many geophysicists were trying to determine the structure of the Earth through the new science of seismology. A Russian geophysicist, Leonid Leybenzon, was the first to publish a paper in 1910, showing that seismic velocities suggest a fluid core. Unfortunately, this article was unknown outside of Russia until after 1950. Oldham, Wiechert, and Gutenberg contributed significantly to the discovery of the Earth's core, but it is Harold Jeffreys who must be credited with the discovery of the core due to his success in

convincing the scientific community.

In 1925, Gutenberg published a monograph describing six methods of finding the rigidity of the Earth:

1. Ocean tides.
2. Displacement of the vertical by solar and lunar attraction.
3. Effect of the Earth's deformation on gravity.
4. Chandler wobble.
5. Speed of seismic waves.
6. dependence of theoretical stability on rigidity at the centre.

This work demonstrated that all criteria, except for speed of seismic waves and apparent inability of the core to transmit shear waves, led to a conclusion of a high rigidity of the core. Gutenberg therefore argued that the apparent inability of the core to transmit shear waves must be explained by a phenomenon other than the core being liquid.

In June 1926, Jeffreys published a paper *The Rigidity of the Earth's Central Core*. In this paper, Jeffreys showed that the average rigidity of the Earth was much smaller than the rigidity of the mantle, meaning the Earth must have a core with a very low rigidity. In order to agree with the Chandler wobble and tidal observations, Jeffreys showed that the change of state from solid to liquid happened at the same time as the change in chemical composition from stone to iron. Jeffreys successfully demonstrated that all evidence mentioned by Gutenberg could be explained by a fluid core model. It is important to note that the S wave shadow zone was not the determining factor in the discovery of fluidity of the Earth's core; rather, it was one of many pieces of evidence that were needed.

Interestingly enough, it was the seismological shadow zone for arcual distances of 105° to 142° that lead Inge Lehmann, a Danish seismologist, to suggest that

the Earth has an inner core. The shadow zone is created by the refraction of waves as they travel through the Earth; waves that just miss striking the Earth's core are refracted up to 105°, and waves that enter the Earth's core are refracted downward in the slower medium making the lowest angle of emergence and focal point of 142°. Any waves found at arcual angles slightly greater than 105°, or slightly less than 142° were attributed to diffraction and the mantle-core interface. Studying compressional waves with less than the focal point of 142° led Lehmann to propose that the Earth had an inner core of radius 0.2205 R (approximately 1400 km) reflecting the P waves. While there were disagreements amongst geophysicists about the transition between the outer and inner core and their velocity differences, it was quickly agreed upon by the geophysical community that there was indeed an inner core. Solidity of the inner core was theorized in 1940 by Francis Birch, however, confirmation of the solidity of the inner core was based on cumulative work by many geophysicists over three decades [5].

Chapter 2

Hookean solids and anisotropy

[1] A Hookean solid is represented by a fourth-rank tensor that linearly relates stress and strain:

$$\sigma_{ij} = \sum_{k=1}^{3}\sum_{\ell=1}^{3} c_{ijk\ell}\varepsilon_{k\ell}, \qquad i,j \in \{1,2,3\}\,,$$

where σ_{ij} is the stress tensor, $c_{ijk\ell}$ is the elasticity tensor, and $\varepsilon_{k\ell}$ is the strain tensor. The Hookean solid defined by the elasticity tensor, $c_{ijk\ell}$, and mass density can be used as a model for physical materials in quantitative seismology. The elasticity tensor representing a solid can exhibit different symmetries, which can be representative of different material properties. There are eight symmetry classes of Hookean solids [3,6]. The relationships among the symmetry classes are shown in Figure 2.1. Due to the partial ordering of the symmetry classes, not all are directly relatable. Each symmetry class is characterized by its symmetry group, which consists of orthogonal transformations of $\mathbb{R}^3$ that preserve tensor c. The largest group is the group of all orthogonal transformations, $O(3)$, which determines the isotropic symmetry class. The symmetry groups of other classes are subgroups of $O(3)$.

In studying anisotropy of the inner core, two symmetry classes were used: isotropic and transversely isotropic. The isotropic elasticity class has the highest

[1] This section is based on Chapters 5, 6, 8, and 9 from *Waves and Rays in Elastic Continua* [17]

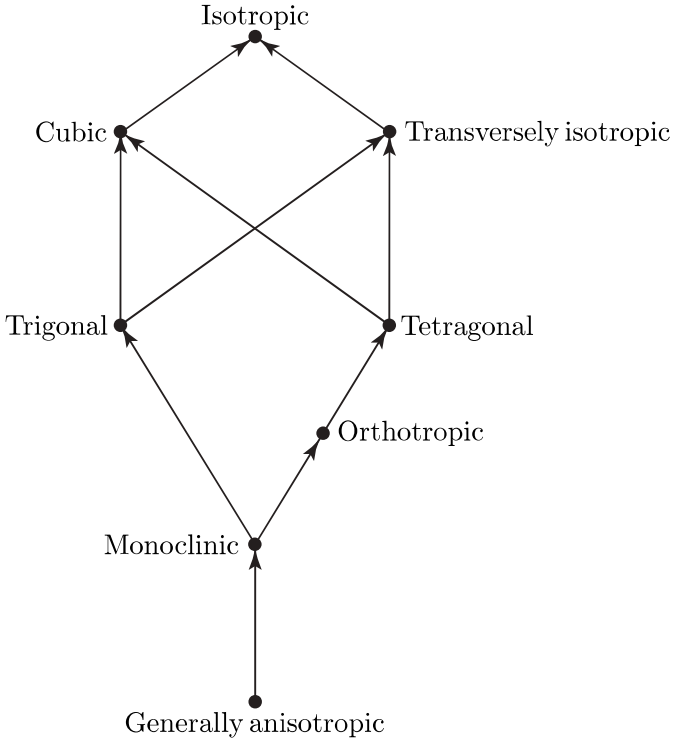

Figure 2.1: Relations among symmetry classes. Arrows show the relations between the subgroups of symmetries, with lower forms of symmetry at the bottom and higher forms of symmetry at the top. *From Waves and Rays in Elastic Continua* p.176 [17] .

form of symmetry and its two independent parameters can be represented in a matrix as[2],

$$\boldsymbol{C_{ISO}} = \begin{bmatrix} C_{11} & C_{11}-2C_{44} & C_{11}-2C_{44} & 0 & 0 & 0 \\ C_{11}-2C_{44} & C_{11} & C_{11}-2C_{44} & 0 & 0 & 0 \\ C_{11}-2C_{44} & C_{11}-2C_{44} & C_{11} & 0 & 0 & 0 \\ 0 & 0 & 0 & C_{44} & 0 & 0 \\ 0 & 0 & 0 & 0 & C_{44} & 0 \\ 0 & 0 & 0 & 0 & 0 & C_{44} \end{bmatrix}.$$

The transversely isotropic elasticity class is highly symmetric and, as illustrated in Figure 2.1, can be considered a step below isotropy, shared with the cubic

[2]The relation between the two-index, C_{mn}, and four-index, c_{ijkl}, notation is provided by Voigt's formula, e.g. *Waves and Rays in Elastic Continua* p.95 [17]

elasticity class. In its natural coordinate system, a transversely isotropic tensor has rotational invariance about one axis. Its five independent parameters can be expressed in matrix form as

$$\boldsymbol{C_{TI}} = \begin{bmatrix} C_{11} & C_{12} & C_{13} & 0 & 0 & 0 \\ C_{12} & C_{11} & C_{13} & 0 & 0 & 0 \\ C_{13} & C_{13} & C_{33} & 0 & 0 & 0 \\ 0 & 0 & 0 & C_{44} & 0 & 0 \\ 0 & 0 & 0 & 0 & C_{44} & 0 \\ 0 & 0 & 0 & 0 & 0 & \frac{C_{11}-C_{12}}{2} \end{bmatrix}.$$

2.1 Isotropic velocity

The velocity of a P wave in isotropic media is

$$v = \sqrt{\frac{C_{11}}{\rho}}, \tag{2.1}$$

where wave velocity v is equal to ray velocity V due to the independence of isotropic velocity with respect to direction.

2.2 Transversely isotropic velocity

In transversely isotropic media, wavefront velocities and ray velocities vary with direction. Wavefront velocity is the velocity of wavefront propagation, and ray velocity is the velocity of propagation along the ray path. Ray velocities vary with ray angle, the angle between the axis of symmetry and the tangent to the direction of ray propagation. Wave velocities are a function of wavefront angle, the angle between the axis of symmetry and the normal vector to the direction of wave propagation. Only at directions when the wavefront normal vector and the ray tangent vector are equal to each other does the ray velocity equal the wave

velocity; therefore, only in directions parallel and perpendicular to the symmetry axis does $v = V$.

2.2.1 Wavefront velocity

Quasi P wave wavefront velocity in transversely isotropic media is

$$v_{qP}(\boldsymbol{n}) = \sqrt{\frac{(C_{33} - C_{11})n_3^2 + C_{11} + C_{44} - \sqrt{\Delta}}{2\rho}}, \tag{2.2}$$

where Δ, the discriminant, is

$$\Delta \equiv \Big[(C_{11} - C_{33})n_3^2 - C_{11} - C_{44}\Big]^2 - 4\Big[C_{33}C_{44}n_3^4$$

$$-\Big[2C_{13}C_{44} - C_{11}C_{33} + C_{13}^2\Big]n_3^2\Big(1 - n_3^2\Big) + C_{11}C_{44}\Big(1 - n_3^2\Big)^2\Big],$$

and n_3 is the orientation of the wavefront normal $\boldsymbol{n}$ with respect to the rotation-symmetry axis (x_3).

Taking the x_3 axis to be the axis of symmetry, the wavefront velocity traveling along the axis of symmetry corresponds to $n_3 = 1$, which results in

$$v_z = \sqrt{\frac{C_{33}}{\rho}} = V_z\,, \tag{2.3}$$

and the wavefront velocity traveling perpendicular to the axis of symmetry, which corresponds to $n_3 = 0$, is

$$v_x = \sqrt{\frac{C_{11}}{\rho}} = V_x\,. \tag{2.4}$$

2.2.2 Ray velocity

In general, there is not a closed-form expression for ray velocities in transversely isotropic media. Calculating ray velocity as a function of ray angle is computationally intensive.

Ray velocity as a function of wavefront angle and wavefront velocity can be shown to be,

$$V(\vartheta) = \sqrt{[v(\vartheta)]^2 + \left[\frac{\partial v(\vartheta)}{\partial \vartheta}\right]^2}\,, \tag{2.5}$$

and the ray angle as a function of wavefront angle and velocity can be shown to be,

$$\tan\theta = \frac{\tan\vartheta + \frac{1}{v}\frac{\partial v}{\partial \vartheta}}{1 - \frac{\tan\vartheta}{v}\frac{\partial v}{\partial \vartheta}}\,.$$

Traveltime measurements between a point source and point receiver correspond to ray velocities, not wavefront velocity.

A closed form ray velocity expression is known only for an elliptical velocity dependence, namely,

$$V(\theta) = V_z\sqrt{\frac{1+\tan^2(\theta)}{1+(\frac{V_z}{V_x})^2\tan^2(\theta)}}\,, \tag{2.6}$$

where $V(\theta)$ is the ray velocity in the direction θ measured from the vertical (symmetry) axis, V_z is the ray velocity in the vertical direction, and V_x is the horizontal ray velocity.

2.3 Anisotropic parameters

To completely describe an isotropic Hookean solid only two elasticity parameters are required, C_{11} and C_{33}. Also, due to the rotation invariance of isotropy no parameters are required for orientation in three dimensions. A total of seven parameters are needed to describe a transversely isotropic Hookean solid; five elasticity parameters, $C_{11}, C_{12}, C_{13}, C_{33}, C_{44}$, and two parameters for orientation such as Euler angles.

P waves in isotropic Hookean solids require one elasticity parameter, C_{11} for description. Quasi P waves in transversely isotropic Hookean solids require four elasticity parameters for description, C_{11}, C_{33}, C_{13}, and C_{44}, along with one parameter for orientation; n_3 in expression (2.2). The elliptical velocity expression needs

two elasticity parameters for description, C_{11} and C_{33}, where $V_z = \sqrt{C_{33}/\rho}$ and $V_x = \sqrt{C_{11}/\rho}$, and one for orientation; θ in expression (2.6).

Chapter 3

Inner core anisotropy

Two types of seismological data are used for studying the inner core; body waves, and normal modes. Body waves at short periods ranging in frequency between 0.5 Hz - 1.5 Hz with a dominant frequency of 1 Hz are observed from earthquakes of magnitude m_b 5.5 or greater [4]. Normal modes are standing waves that are created from very large scale earthquakes; they are very low frequency events, with frequencies less than 10 mHz. They are sensitive to velocity, attenuation, and density, providing the clearest data to tell us about the density of the inner core [4].

There have been many papers published on anisotropy of the inner core since 1986. The earliest theories suggested that the inner core displayed cylindrical anisotropy with a symmetry axis aligned with the axis of rotation [15] [26]. The transversely isotropic symmetry class is sometimes referred to as cylindrical anisotropy, because the way the magnitude of velocity varies with ray angle can be geometrically thought of as a cylinder.

A second theory is that of hemispherical variations, with the eastern hemisphere largely isotropic, and the western hemisphere being strongly anisotropic [19] [21]. A third theory is of an innermost inner core [11] [22] displaying a different anisotropy from the upper layer.

Currently, some of the most compelling research [8] shows that the outer 60-80 kilometres of the inner core is isotropic with the inner part displaying 3-4% anisotropy and hemispherical variation of the anisotropy. A possible source of the anisotropy could be iron crystal alignment, believed to be of the hexagonally close-packed crystal system with some positioned during solidification and others from deformation.

3.1 Anisotropy of the Inner core from body waves

The 1986 paper by Morelli, Dziewoński, and Woodhouse *Anisotropy of the inner core inferred from PKIKP traveltimes* [15] was the first paper to introduce the concept of inner core anisotropy. Using PKP and PKIKP traveltimes for distances of 110° to 180° from Bulletins of the International Seismological Centre from 1964 to 1982, subsets of data were created and examined leading the authors to suggest an anisotropy with a cylindrical symmetry aligned with the axis of rotation.

There are many types of body waves theorized to be present in the inner core. Compressional waves that are believed to be present in the inner core are PKIKP, PKIIKP, pPKIKP, pPKIIKP, sPKIKP, sPKIIKP, SKIKP, and more exotic inner core phases. There are also many shear phases believed to be present in the inner core such as PKJKP, SKJKS, SKJKP, pPKJKP, etcetera. For a review of the naming convention associated with body-wave phases, see Appendix A.

Aside from PKIKP body waves, inner core phases are very difficult to observe. As of late 2014 there have only been three verified observations of inner core shear waves by fluid inner core synthetic tests, although more unverified accounts have been suggested. Exotic inner core waves are very low amplitude, and in the case of shear waves, can be highly attenuated; they are difficult to observe in single seismograms. The use of stacking and synthetic seismograms are needed to observe these lower amplitude body waves [23].

3.2 Anisotropy of the Inner core from normal modes

In the same issue of Geophysical Research Letters that featured *Anisotropy of the inner core inferred from PKIKP traveltimes*, there was a paper by Woodhouse, Giardini, and Li, published *Evidence for inner core anisotropy from free oscillations* [26]. This paper examined anomalous splitting of free oscillations, ruling out mantle and outer core heterogeneity as the source of the split modes. It is argued that the only possible source for the observed splitting of normal modes comes from an inner core anisotropy. Examining the special case of cylindrical anisotropy with the symmetry axis aligned with the axis of rotation, they show that observations can closely be matched with modelled data. They note that cylindrical anisotropy does not match higher degree split modes and that there is likely a better model of inner core anisotropy than cylindrical anisotropy to fit the observations.

Chapter 4

Modelling

In order to study the accuracy and number of measurements required to determine anisotropy in a spherical body with properties similar to the inner core, several models were constructed. The three most interesting cases are presented in this thesis. The physical properties of the models were based on values from the Preliminary Reference Earth Model (PREM). A description of PREM is given in Appendix E.

The anisotropic qP velocity within a transversely isotropic body was approximated using the elliptical velocity function (expression 2.6),

$$V(\theta) = V_z \sqrt{\frac{1 + \tan^2(\theta)}{1 + (\frac{V_z}{V_x})^2 \tan^2(\theta)}} \,,$$

where $V(\theta)$ is the ray velocity in the direction θ measured from the vertical (symmetry) axis, V_z is the ray velocity in the vertical direction, and V_x is the horizontal ray velocity. The average inner core velocity, $V_{IC}(x)$, taken from PREM (see Table E1) was used as the ray velocity in the horizontal direction,

$$V_x \approx \frac{1}{b-a} \int_a^b V_{IC}(x)\, \mathrm{d}x \,, \tag{4.1}$$

where, b, the normalized radius of the inner core, is 1221.5/6371 km, and a, the

centre of the Earth is zero. The vertical ray velocity (V_z) was set as 5% faster than the horizontal velocity.

The model created represents an anisotropy on the scale of 5%; this is similar to values suggested to be reasonable by Duess, 2014 [8]. The use of the elliptical velocity function in the modelling serves several purposes, but the main reason is lack of information about mechanical properties of the inner core. Without the ability to measure the elasticity parameters C_{13} and C_{44}, and due to their independence, the complete form of the quasi-P wave velocity expression (expression (2.2)) was unusable.

Measurements of mechanical properties and anisotropy of iron crystals or similar metals of various packing phases possibly present in the inner core have been performed, however, there is large variability of measurements with pressure and temperature [1, 13, 18]. It was shown by Backus [2] that by the small scale properties do not reflect the measurements of anisotropy in long waveforms; therefore, it was decided that attempting to use iron crystal mechanical properties to create an effective medium for the inner core was beyond the scope of this project.

The use of the elliptical velocity function expression 2.6 to represent qP ray velocities eliminates some computational difficulties; there is not a closed form equation for qP rays in transversely isotropic media. There is a closed form equation for qP wavefront velocities and relations between wavefront and ray velocities, expression 2.5; therefore, ray velocity can be calculated through a difficult computational process. The elliptical velocity approximation, however, simplifies the computational process. It is important to note that, in general, variation in qP waves or rays with angle in transversely isotropic media do not follow an elliptical pattern, but given assumptions and estimations already present in the modelling, and the similarity between a general transversely isotropic wavefront and its elliptical counterpart, it is a reasonable approximation.

The physical properties for the considered transversely isotropic body are

$$V_z = 11.76\,\text{km/s}, \;\; V_x = 11.2\,\text{km/s},$$

and the radius is $r = 1200$ km. Traveltime calculations are performed by setting hypothetical source and receiver locations on the circumference. In reality, it is impossible to set up sources and receivers on the circumference of the inner core, however, this approach is similar to the concept of layer stripping. We assume that we can successfully resolve the contributions to traveltime measurements from the surface through to the Inner core boundary; hencethe only properties we are trying to resolve come from the inner core itself.

4.1 Case 1: Full sampling of ray angles

The first case examined was created to test how sampling of a wide range of ray angles and numerous traveltime measurements with little errors present in the data allow for distinguishing between isotropic and transversely isotropic models. The model was constructed with the source located on the axis of symmetry and receivers located at arcual distances ranging from 10° to 180° incrementally by 10° arcual distance. This corresponds to sampling of ray angles (θ) between 0-85° as shown in Figure 4.1.

4.2 Case 2: Data Scarcity - Near-horizontal ray angles

The second case examined was used to study the effects of data sparsity in resolving anisotropy. If sampling near horizontal ray angles, there is the greatest difference between the isotropic and transversely isotropic velocities based on the modelling

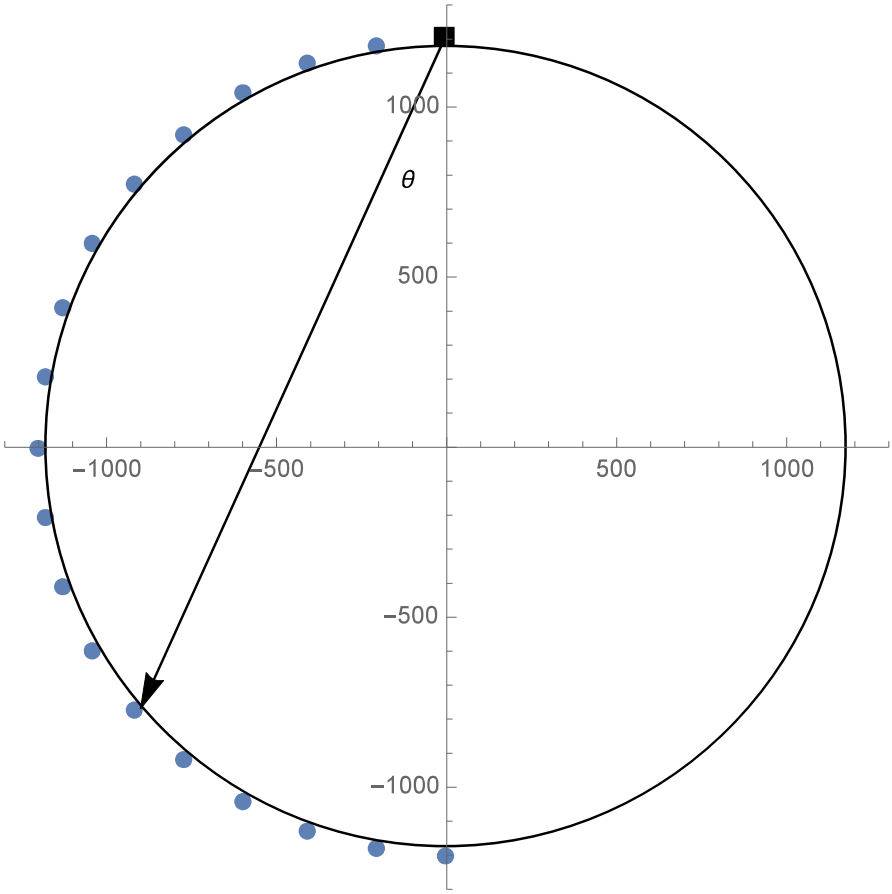

Figure 4.1: Case 1: Source and receiver locations. The source is shown as a black square and the receivers are shown as blue circles. The ray angle (θ) is measured from the axis of symmetry (vertical axis) as shown for one ray path.

parameters. The source is set on the horizontal axis (axis perpendicular to the axis of symmetry) and the six receivers have ray angles varying from 75° to approximately 100° as seen in Figure 4.2. Table 4.2 displays the distances between source and receivers, ray angles, and velocities used in the forward modelling.

4.3 Case 3: Data Scarcity - Intermediate ray angles

The third examined case was used to study the effects of data sparsity if the ray angles are at intermediate values, and therefore, a large variation of velocities in the case. The source was set at 50° arcual distance from the horizontal axis and

Receiver Number	Distance (km)	Ray Angle (Degree)	Velocity (km/s)
1	209.174	85	11.2040
2	416.756	80	11.2157
3	621.166	75	11.2350
4	820.848	70	11.2614
5	1014.28	65	11.2942
6	1200.00	60	11.3325
7	1376.58	55	11.3753
8	1542.69	50	11.4215
9	1697.06	45	11.4698
10	1838.51	40	11.5186
11	1965.96	35	11.5666
12	2078.46	30	11.6122
13	2175.14	25	11.6538
14	2255.26	20	11.6901
15	2318.22	15	11.7198
16	2363.54	10	11.7419
17	2390.87	5	11.7554
18	2400.00	0	11.76 00

Table 4.1: Distances between source and receivers, ray angles, and velocities used in Case 1, where receiver 1 is the top receiver and receiver 18 is the bottom receiver.

Receiver Number	Distance (km)	Ray Angle (Degree)	Velocity (km/s)
1	2363.54	99.9227	11.2155
2	2390.87	94.9244	11.2038
3	2400.00	90	11.2000
4	2390.87	85	11.2040
5	2363.54	80	11.2157
6	2318.22	75	11.2350

Table 4.2: Distances between source and receivers, ray angles, and velocities used in Case 2, where receiver 1 is the top receiver and receiver 6 is the bottom receiver.

the six receivers were set so that the ray angles varied from 35° to 60° as shown in Figure 4.3. Table 4.3 displays the distances, ray angles, and velocities used in the forward modelling. While the range of ray angles is the same as Case 2 ($\approx 25°$), the distances and velocities vary more significantly in Case 3.

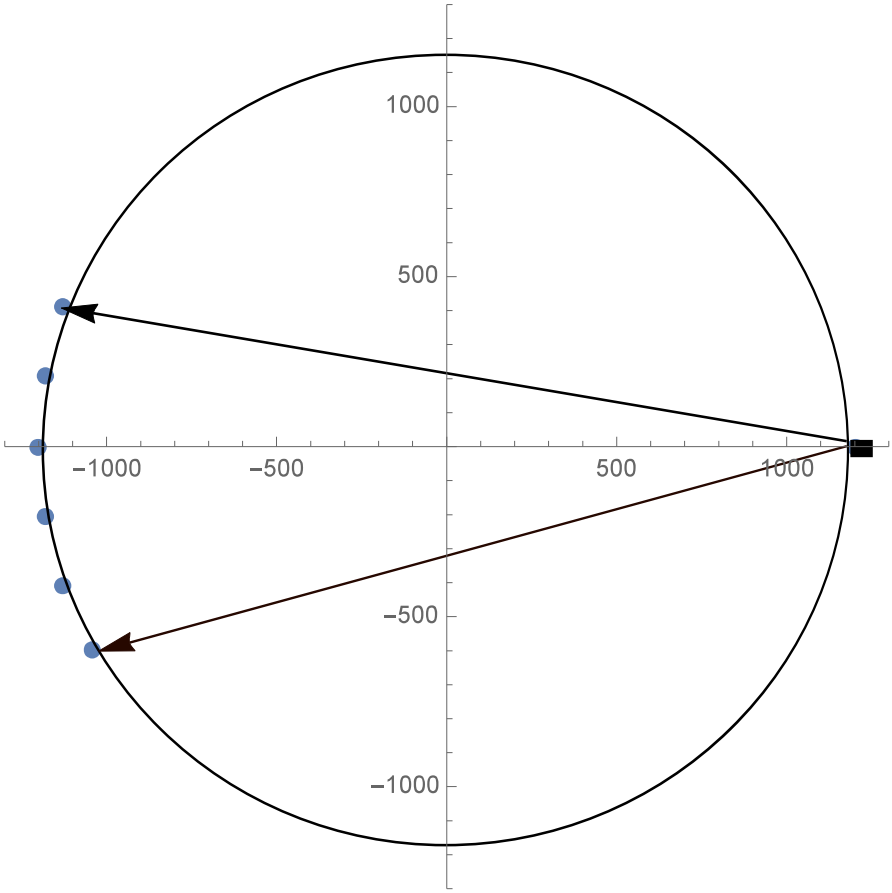

Figure 4.2: Case 2: Source and receiver locations. The source is shown as a black square and the receivers are shown as blue circles. The ray paths shown highlight the low variation in ray angle measured from the vertical axis.

Receiver Number	Distance (km)	Ray Angle (Degree)	Velocity (km/s)
1	2255.26	60	11.3325
2	2318.22	55	11.3753
3	2363.54	50	11.4215
4	2390.87	45	11.4698
5	2400.00	40	11.5186
6	2390.87	35	11.5666

Table 4.3: Distances between source and receivers, ray angles, and velocities used in Case 3, where receiver 1 is the top receiver and receiver 6 is the bottom receiver.

4.4 Forward problem

For the cases under consideration, the forward problem of traveltime calculations was addressed. For this, the distances between the source and receivers and the

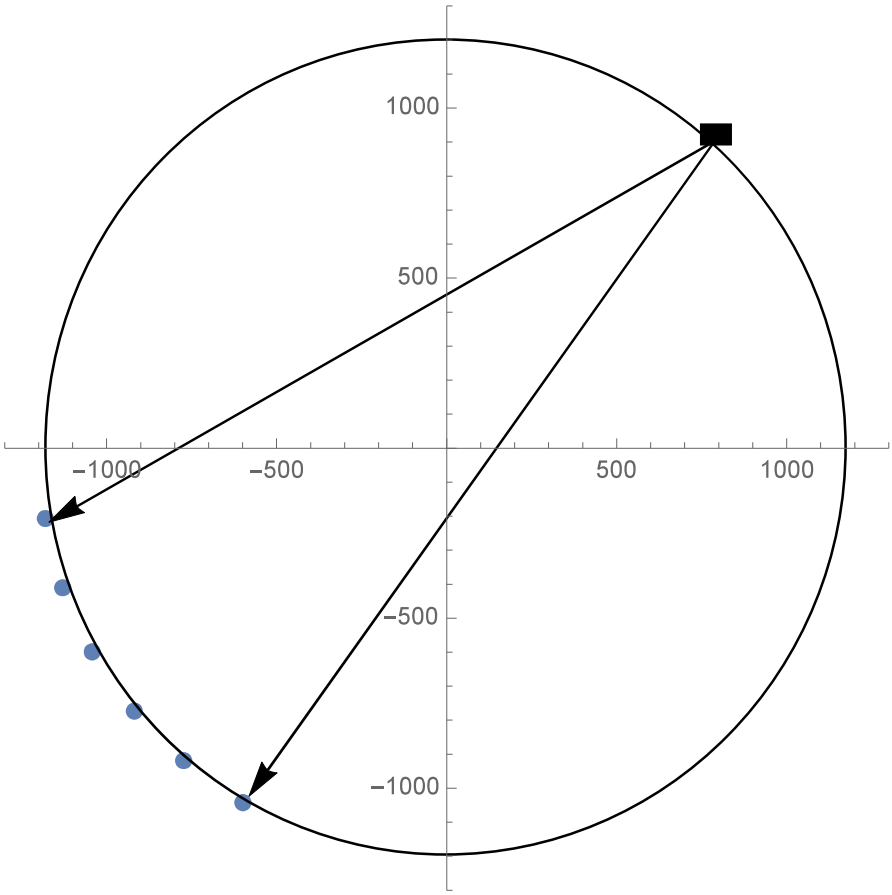

Figure 4.3: Case 3: Source and receiver locations. The source is shown as a black square and the receivers are shown as blue circles. The ray paths shown highlight the low variation in ray angle measured from the vertical axis.

ray angles were computed for each of the three cases. Then, traveltimes with random normally distributed errors were calculated for each receiver position. The errors present in the traveltime values represent possible errors that could occur from inability to fully resolve contributions from outer layers of the Earth, errors in traveltime picking, and measurement inaccuracies. The number of traveltime measurements and percentage of random errors allowed into the data is displayed in Table 4.4. Case 1 has more traveltime measurements than Case 2 or Case 3 because it examines an ideal sampling case, while Cases 2 and 3 examine more realistic cases of dealing with data scarcity.

	Traveltime Measure-ments	Errors
Case 1	10	±1%
Case 2	3	±4%
Case 3	3	±4%

Table 4.4: Number of traveltime measurements and percentage of randomly normally distributed error allowed into the traveltime measurements per case.

4.5 Inverse problem

Two statistical tests were used for examining the inverse problem: the KS test, and BIC, explained in appendices B and D, respectively. Different approaches were required to prepare the data for the KS test and BIC. The KS test required the calculation of isotropic traveltime results at the receiver locations, and the BIC required an attempt to fit an isotropic and an elliptic velocity function to the traveltime results generated from the forward problem.

The initial steps of the inverse problem, preparing data for BIC and the KS test, were the same. An average of the traveltime calculations from the forward problem were calculated for each receiver,

$$t_{avg} = \frac{\sum_{i=1}^{n} t_i}{n},$$

where n is the number of traveltime measurements. Throughout this averaging it was assumed that the average of the random normally distributed errors present in the data remains normally distributed throughout the averaging process.

Two minimization functions were created to obtain the elliptically dependant velocity parameters, V_z and V_x, and the isotropic velocity, V_{iso}. The elliptical-

velocity minimization function is

$$f(V_z, V_x) = \sum_{i=1}^{n} \left| t_i - \frac{D_i}{V_z \sqrt{\frac{1+\tan^2(\theta_i)}{1+(\frac{V_z}{V_x})\tan^2(\theta_i)}}} \right| , \tag{4.2}$$

where t_i, D_i and θ_i are known, and V_x and V_z are calculated to minimize the value of $f(V_x, V_z)$ through the *Mathematica* NMinimize function. The elliptical velocity function has three parameters, V_x, V_z and θ. However, due to the fact that in homogeneous media rays are straight, the ray angles are known, and optimization is not required for θ.

Similarly, the isotropic velocity minimization function is

$$f(V_{iso}) = \sum_{i=1}^{n} \left| t_i - \frac{D_i}{V_{iso}} \right| , \tag{4.3}$$

where the function is minimized following the same procedure. With the values of V_{iso}, V_z and V_x computed, BIC can be used to test if there is sufficient information to accept a more complicated, transversely isotropic model, as opposed to the simpler, isotropic model.

The KS test works by comparing two data sets to determine the likelihood that errors caused the observed difference between datasets, as opposed to the datasets being derived from separate distributions. In order to test if there was sufficient information to determine if the model was better explained by isotropy or transverse isotropy, isotropic traveltimes needed to be calculated for each receiver position.

In order to calculate isotropic traveltimes to compare to the forward modelled traveltimes with errors present in the data, the errors in the transversely isotropic traveltimes had to be examined. This was done by calculating the standard devi-

ation of each receiver's traveltime values,

$$\sigma = \sqrt{\frac{1}{n}\sum_{i=1}^{n}(t_i - t_{avg})^2}\,.$$

With the standard deviation calculated, isotropic traveltimes were then determined using the distances and ray angles already calculated for the forward models, along with the minimized isotropic velocity and random normally distributed errors of up to plus or minus three times the standard deviation. Allowing up to three times the standard deviation as errors in the traveltime calculations was done because approximately 99.7% of the data assuming normal distribution falls within three standard deviations of the average value. This approach also allowed for examination of how the ability to predict errors in the data affects our ability to choose models. An equal number of isotropic and transversely isotropic traveltimes were calculated for each receiver position, and then isotropic and transversely isotropic traveltimes were compared using the KS test.

The *Mathematica* code for both the forward and inverse modelling for Case 1 is shown in Appendix F. Modifications of the code presented are easily done for Case 2 and Case 3.

Chapter 5

Results

In this section, the results of forward and inverse modelling are presented for each case. Firstly the forward modelled and isotropic traveltimes are compared, along with the range of errors allowed for the isotropic traveltimes. The KS test results are presented, where a p-value of greater than 0.05 is interpreted as differences in the data set originating from errors present in the data, rather than inherently different models. Secondly, the minimization velocity parameters and the outputs of the BIC are presented. The lower value of BIC is interpreted to be the preferred model. Due to the prior knowledge that the models are different, when isotropy is picked from the KS test or BIC, the interpretation is that there has been insufficient sampling or too much error present in the data.

5.1 Case 1: Full sampling results

The isotropic velocity parameters and elliptically dependant velocity parameters calculated from the minimization functions are

$$V_{iso} = 11.6348\,\mathrm{km/s}$$

and

$$V_z = 11.7556\,\text{km/s},\ V_x = 11.2075\,\text{km/s},$$

respectively. The results of the transversely isotropic minimization are close to the input values of the forward model. Errors allowed into the isotropic traveltimes are shown in Table 5.1. The errors that were calculated from the forward model are greater than the errors introduced into the forward model. The larger errors are due to sample size; with few measurements the errors calculated can be strongly influenced by outsider values.

Receiver Number	Errors	Receiver Number	Errors
1	±1.79915%	10	±1.5368%
2	±1.69682%	11	±1.4781%
3	±0.944957%	12	±1.08094%
4	±1.37367%	13	±2.13532%
5	±1.72387%	14	±1.75678%
6	±1.61903%	15	±1.45677%
7	±2.37716%	16	±1.6914%
8	±2.16731%	17	±2.05096%
9	±1.60246%	18	±1.50989%

Table 5.1: Amount of random normally distributed traveltime errors allowed into isotropic traveltime measurements.

Receiver Number	p-value	Receiver Number	p-value
1	0.0000108251	10	0.000216502
2	0.0000108251	11	0.00205677
3	0.0000108251	12	0.0123406
4	0.0000108251	13	0.167821
5	0.0000108251	14	0.417524
6	0.0000108251	15	0.417524
7	0.0000108251	16	0.417524
8	0.0000108251	17	0.167821
9	0.0000108251	18	0.417524

Table 5.2: Results of Kolmogorov-Smirnov test for Case 1.

The traveltime values calculated from the elliptical velocity forward modelling

and isotropic inverse modelling are displayed in Figure 5.1. It is apparent that as the ray angle decreases, the similarity between isotropic and transversely isotropic traveltimes increases. Based on the velocities input into the forward model and isotropic model it makes sense that there is an increase in traveltime similarity with a decrease in ray angle. The results of the KS test comparing the isotropic traveltimes and transversely isotropic traveltimes are shown in Table 5.2. Based on the information available for the KS test, 0.0123406 is the minimum p-value that can be calculated for Case 1. The majority of the KS test p-values predict that the traveltimes calculated from the forward modelling do not come from an isotropic model; however, as the ray angle decreases, the similarity between the isotropic velocity and the elliptical velocity increases, thereby making the KS test predict that the forward modelled traveltimes are isotropic at low ray angles.

The calculated velocity parameters result in BIC values,

$$BIC(Iso) = 9.21709$$

and

$$BIC(TI) = -59.5079\,.$$

In this case, BIC clearly chooses the elliptical velocity dependence model as the preferred model.

5.2 Case 2: Data Scarcity - Near-horizontal ray angles results

The second case examined has ray paths that are near perpendicular to the axis of symmetry. Minimization of the forward modelled traveltimes resulted in

$$V_{iso} = 11.2775\,\mathrm{km/s}\,,$$

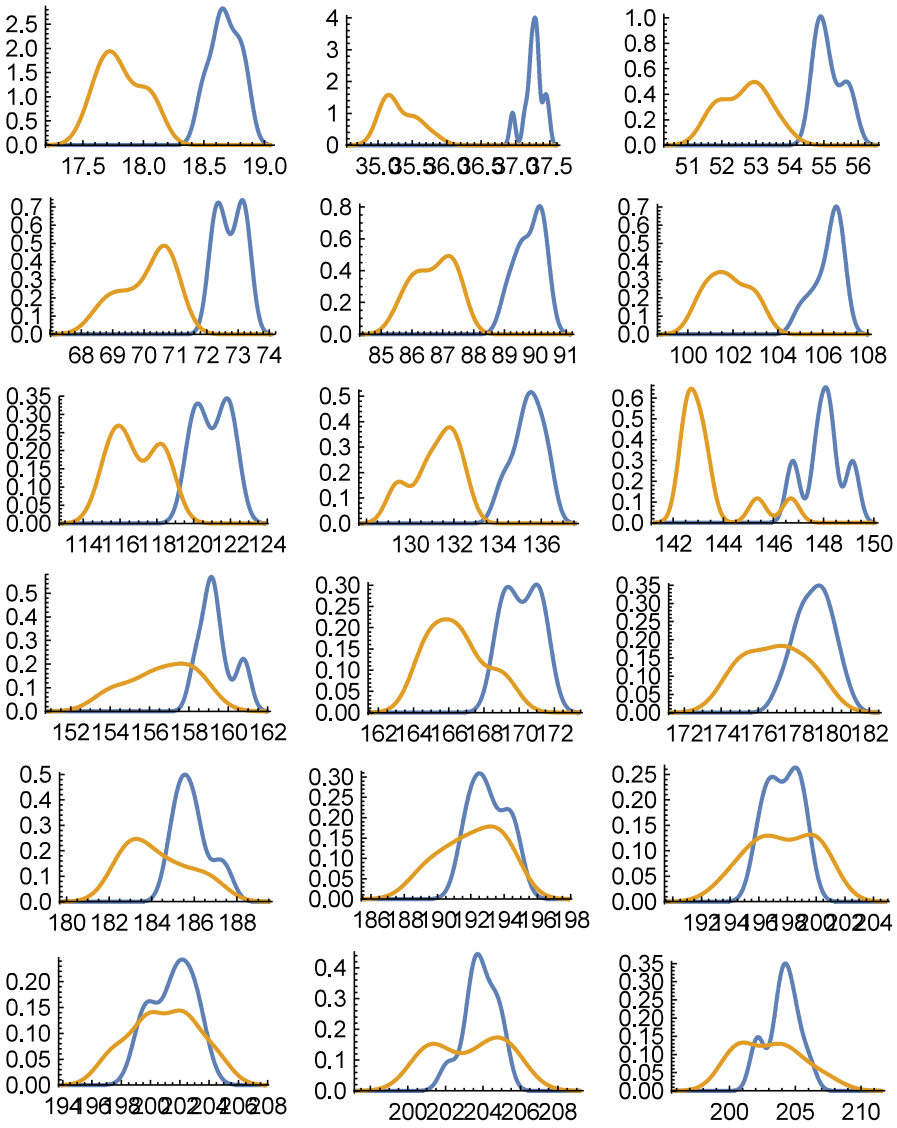

Figure 5.1: Histograms of Case 1 traveltime results. Isotropic traveltimes are shown in yellow and transversely isotropic traveltimes are shown in blue. Receiver positions increase from left to right and top to bottom, with receiver 1 being at the top left and receiver 18 being at the bottom right.

for the isotropic velocity, and

$$V_z = 11.3126\,\text{km/s}, V_x = 11.2772\,\text{km/s},$$

for the elliptical velocity parameters. The calculated V_z is smaller than the V_z from the forward model. The range of random errors allowed into the isotropic traveltimes are displayed in Table 5.3. The errors predicted from the forward

model are significantly larger than the errors introduced into the forward model.

Receiver Number	Errors	Receiver Number	Errors
1	±6.26028%	4	±11.5545%
2	±13.143%	5	±9.4062%
3	±10.4336%	6	±10.8732%

Table 5.3: Range of random normally distributed errors allowed into Case 2 isotropic traveltime results.

Three traveltimes were calculated for each receiver; traveltime results are shown in Figure 5.2. The forward modelled traveltimes tend to be similar to the isotropic traveltimes; overall, half of the forward modelled traveltimes are faster than the isotropic traveltimes. Examining the variation between the isotropic and elliptically velocity dependant traveltimes, it appears that the variations are caused by random errors. This makes sense because the input isotropic velocity value is quite close to the minimized horizontal velocity value, and the ray paths being sampled are near horizontal. The KS test results displayed in Table 5.4 show that there is not sufficient information to distinguish the two models. Therefore, isotropy would be picked as the most likely source model.

Receiver Number	p-value	Receiver Number	p-value
1	0.1	4	1
2	0.6	5	0.6
3	0.6	6	0.6

Table 5.4: Results of Kolmogorov-Smirnov test for Case 2.

The BIC results of the minimized functions are

$$BIC(Iso) = 18.7867$$

and

$$BIC(TI) = 22.3601\,.$$

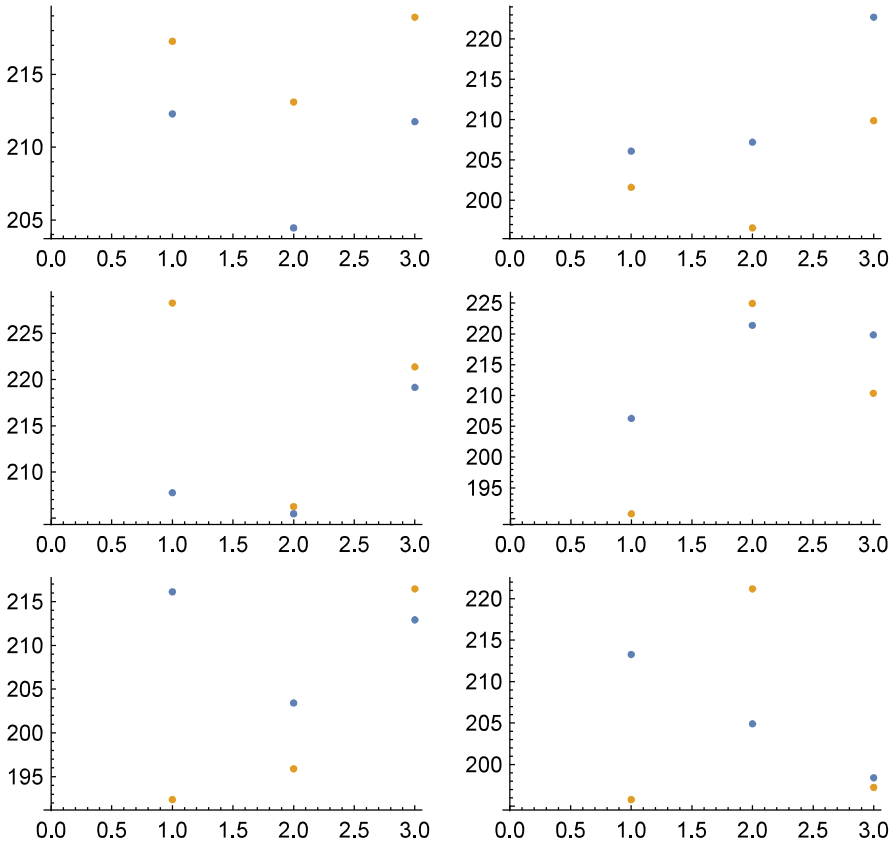

Figure 5.2: Scatter plots of Case 2 traveltime results. Isotropic traveltimes are shown in yellow and transversely isotropic traveltimes are shown in blue. Receiver positions increase from left to right and top to bottom, with receiver 1 being at the top left and receiver 6 being at the bottom right. The Y-axis shows traveltime in seconds.

BIC chooses the isotropic model as the preferred source model based on the information available. The BIC values are close together, so a great deal of confidence cannot be placed in the results.

5.3 Case 3: Data Scarcity - Intermediate ray angle results

The minimization results for Case 3 resulted in an isotropic velocity of

$$V_{iso} = 11.3854\,\mathrm{km/s},$$

and elliptical velocity parameters of

$$V_z = 11.4412\,\text{km/s}, V_x = 11.2739\,\text{km/s}.$$

Compared to the velocities put into the forward model, the isotropic velocity is low. It is, however, intermediate between the calculated V_z and V_x from the elliptical velocity minimization. With the exception of the first and fifth receivers, the amount of random normally distributed errors allowed (see Table 5.5) into the isotropic traveltime calculations were less than allowed into the forward model.

Receiver Number	Errors	Receiver Number	Errors
1	±7.25447%	4	±1.85968%
2	±3.18143%	5	±4.91204%
3	±1.37901%	6	±2.56807%

Table 5.5: Range of random normally distributed errors allowed into Case 3 isotropic traveltime results.

The traveltimes calculated for the forward and inverse problems for Case 3 are displayed in Figure 5.3. Comparing the three traveltimes calculated at each receiver it is noticeable that as the ray angle decreases, and thereby the rays become more vertical there is a change in traveltime relationships between the forward modelled traveltimes and the isotropic traveltimes; the majority of the isotropic traveltimes calculated for the first four receivers are smaller than the forward modelled traveltimes, and the relationship reverses for the last two receivers. The results of the KS test shown in Table 5.6 show that there is not enough information to distinguish between models, meaning that based on the information we have, it should be interpreted that the forward modelled data came from an isotropic model.

The calculated parameters resulted in BIC outputs of

$$BIC(Iso) = 710.157$$

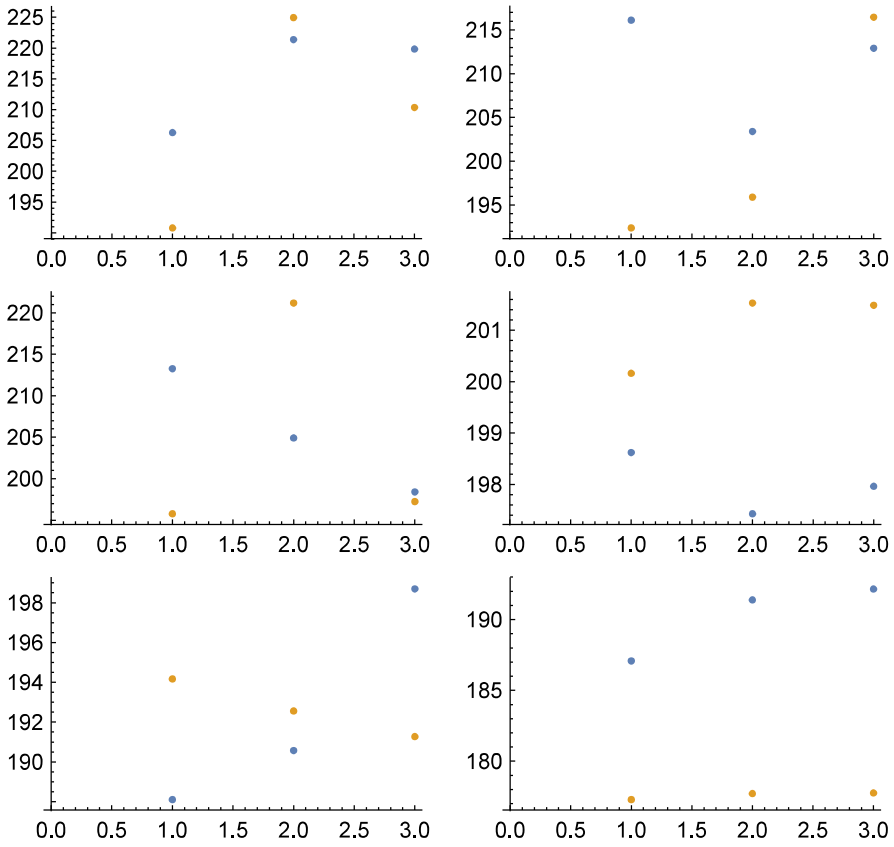

Figure 5.3: Scatter plots of Case 3 traveltime results. Isotropic traveltimes are shown in yellow and transversely isotropic traveltimes are shown in blue. Receiver positions increase from left to right and top to bottom, with receiver 1 being at the top left and receiver 6 being at the bottom right. The Y-axis shows traveltime in seconds.

and

$$BIC(TI) = 682.705\,.$$

BIC favours the elliptical velocity model as the better model out of the two that were compared. This means that while there does not appear to be enough information to distinguish between models at specific receiver locations through the KS test, overall, there is sufficient sampling to choose the more complicated model with BIC.

Receiver Number	p-value	Receiver Number	p-value
1	0.6	4	0.1
2	0.1	5	1
3	0.1	6	1

Table 5.6: Results of Kolmogorov-Smirnov test for Case 3.

Chapter 6

Discussion

As expected, with more measurements and decreasing error, the ability to resolve the underlying source of the measurements increases. This is well demonstrated when comparing all three cases. Case 1 had the smallest errors introduced into the data and the most traveltime measurements; this provided far more confidence in choosing transverse isotropy as the preferred model when using BIC. For Case 3 BIC also chose elliptical anisotropy as the preferred source model, while for Case 2 isotropy was preferred as the source model.

Examining the input velocities for Case 2, as shown in Table 4.2 there is little variation in the velocities and distances for source-receiver pairs in the forward model. This lack of variation is due to the symmetry of the model. Both Case 2 and Case 3 have a 25° range of ray angles; however, unlike Case 2, Case 3 sampling does not cross a symmetry axis, resulting in a larger variation of velocities. This larger variation in velocities results in BIC being able to correctly choose the elliptical model as the the preferred model.

There were not enough traveltimes calculated in Case 2 or Case 3 for the KS test to be useful. The KS test increases in efficiency with more data points; three measurements are not enough to be able to compare data sets accurately. When dealing with statistical tests such as the KS test it is important to recognize the

central limit theorem described in Appendix C. The relevance of the theorem to this study is that with few samples, and errors present in the samples, the overall distribution can be affected by outlying values; however, with increased sampling, the distribution tends to become approximately normally distributed. In frequency based statistical tests such as BIC and the KS test this is very relevant. The ten traveltimes for each receiver location in Case 1 is still low by frequency based standards.

Examining Case 1, the low errors combined with the greater number of traveltime measurements allowed the KS test to be used effectively. The majority of the KS test results showed a p-value of less than 5%, meaning the difference between the data sets likely did not come from errors in the data, and the case is likely not isotropic. As the ray angle increased the KS test results increased the likelihood that the models were isotropic. Examining the forward model velocities and the isotropic velocity, it would be expected that the largest similarities between the datasets would be found near receiver 12 or 13. The KS test results and the traveltime histograms show increasing similarity between data sets as the ray angle increases. This increase in similarity could be used to infer possible orientation of the symmetry axis; however, with increased number of measurements this relationship could change.

There are several extensions of this project that could be undertaken to further study information to establish preference between isotropic and transversely isotropic models. Cases presented in this thesis are just single realizations of the case; with random errors present, outcomes could vary with computation. Studying the results of many realizations of the case (perhaps even hundreds or thousands) could provide insight into the robustness of the statistical tests with the given errors. Modifications of the code could be performed to be representative of vertical seismic profile (VSP) measurements to study applicability to exploration seismology. Additional layering could be introduced into the cases to account for

other seismological zones. Removal of assumptions used in this thesis may provide a more robust model of the inner core.

Chapter 7

Concluding Remarks

The purpose of this study was not to determine whether or not the inner core is anisotropic, but to examine the information required to answer that question. More specifically, the purpose was to quantify the criteria necessary to give a preference to either the isotropic or transversely isotropic model. This was done by examining body-wave traveltime measurements representative of isotropic and transversely isotropic Inner core cases, in the context of errors and sparsity of data.

The more parameters a model has, the more precisely it can be made to fit a data set. The isotropic P wave velocity has one parameter, V. The elliptically dependant velocity expression has three parameters, V_z, V_x and θ. While only two parameters are optimized because θ in a homogeneous medium is predetermined by the source and receiver locations, the penalty term used in BIC is still based on three parameters. Hence, the elliptical velocity model can be made to fit any data set better than the isotropic model. However, this does not mean that the physical body is represented better by an elliptically dependant velocity model. Errors in the data, possibly due to measurement inaccuracy or model inaccuracy, are also accommodated better by a higher-parameter model.

To avoid a hasty and perhaps faulty choice of a model, it is essential to use a criterion that takes these issues into account. Penalties are required for introducing

extra parameters to a model. The penalties introduced by the KS test are related to the number of data points collected, meaning that with insufficient sampling it will not allow a more complicated model to be chosen. BIC directly penalizes additional parameters, with each additional parameter adding to the value of BIC, and the preferred model is the one with the lowest value of BIC.

The cases presented shows that the KS test may not be a suitable statistical test for determining inner core anisotropy due to the unrepeatability of measurements. This does not rule out the applicability of the KS test in studying anisotropy through other geophysical methods. For example, the KS test would be applicable for studying anisotropy through walk-away vertical seismic profiling, where repeatability and number of measurements are not an issue. BIC tests the overall distribution of measurements for a continuum, whereas the KS test only evaluates variation along a single ray path.

BIC is a more robust method for studying anisotropy in the context of the inner core. Despite relatively few traveltime measurements and a large variance of error allowed into the data, $\pm 4\%$, enough sampling allows us to detect change of velocity with direction, and BIC is able to correctly choose the more complicated model as the preferred source model.

Both BIC and the KS test may be used to study anisotropy, however, BIC is more applicable for both global seismology and exploration seismology.

Bibliography

[1] Antonangeli, D., Merkel, S., and Farber, D. L. Elastic anisotropy in hcp metals at high pressure and the sound wave anisotropy of the earth's inner core. *Geophysical Research Letters 33* (2006).

[2] Backus, G. E. Long-wave elastic anisotropy produced by horizontal layering. *Journal of Geophysical Research 67*, 11 (1962), 4427–4440.

[3] Bóna, A., Bucataru, I., and Slawinski, M. A. Material symmetries of elasticity tensors. *The Quarterly Journal of Mechanics and Applied Mathematics 57*, 4 (2004), 583–598.

[4] Bormann, P., Storchak, D. A., and Schweitzer, J. The iaspei standard seismic phase list. *Seismological Research Letters 74*, 6 (2003), 761–772.

[5] Brush, S. G. Discovery of the Earth's core. *American Journal of Physics* (1980).

[6] Chadwick, P., Vianello, M., and Cowin, S. C. A new proof that the number of linear elastic symmetries is eight. *Journal of the Mechanics and Physics of Solids 49* (2001), 2471–2492.

[7] Conover, W. J. *Practical Non-Parametric Statistics*. John Wiley and Sons Inc., 1971.

[8] Deuss, A. Heterogeneity and anisotropy of earth's inner core. *Annual Review of Earth and Planetary Sciences* (2014).

[9] Dziewoński, A. M., and Anderson, D. L. Preliminary reference Earth model. *Physics of the Earth and Planetary Interiors* (1981).

[10] Halley, E. An account of the cause of the change of the variation of the magnetical needle; with an hypothesis of the structure of the internal parts of the earth: as it was proposed to the royal society in one of their late meetings. *Philosophical Transactions 16* (1683-1775), 563–578.

[11] Ishii, M., and Dziewoński, A. M. The innermost inner core of the earth: Evidence for a change in anisotropic behavior at the radius of about 300 km. *Proceedings of the National Academy of Sciences* (2002).

[12] Kass, R. E., and Raftery, A. E. Bayes factors. *Journal of the American Statistical Association 90*, 430 (1995), 773–795.

[13] Liu, J., Alatas, J.-F. L. A., and Bi, W. Sound velocities of bcc-fe0.85 si0.15 alloy at high pressure and temperature. *Physics of the Earth and Planetary Interiors 233* (2014), 24–32.

[14] Marsaglia, G., Tsang, W. W., and Wang, J. Evaluating kolmogorovs's distribution. *Jounal of Statistical Software 8* (2003).

[15] Morelli, A., Dziewonski, A. M., and Woodhouse, J. H. Anisotropy of the inner core inferred from pkikp travel times. *Geophysical Research Letters 13*, 13 (December 1986), 1545–1548.

[16] Schwarz, G. Estimating the dimension of a model. *The Annals of Statistics* (1978).

[17] Slawinski, M. A. *Waves and Rays in Elastic Continua.* World Scientific, 2015.

[18] Steinie-Neumann, G., Stixrude, L., Cohen, R., and Gulseren, O. Elasticity of iron at the temperature of the earth's inner core. *Letters to Nature 413* (2001), 57–60.

[19] Tanaka, S., and Hamaguchi, H. Degree one heterogeneity and hemispherical variation of anisotropy in the inner core from pkp(bc)-pkp(df) times. *Journal of Geophysical Research 102*, B2 (February 1997), 2925–2938.

[20] Tijms, H. *Understanding Probability.* Cambridge University Press, 2012.

[21] Tromp, J. Inner-core anisotropy and rotation. *Annual Review of Earth and Planetary Sciences* (2001).

[22] Wang, T., Song, X., and Xia, H. H. Equatorial anisotropy in the inner part of earth's inner core from autocorrelation of earthquake coda. *Nature Geoscience* (2015).

[23] Waszek, L., and Deuss, A. Observations of exotic inner core waves. *Geophysical Journal International 200*, 3 (2015), 1636–1650.

[24] Weisstein, E. W. Maximum likelihood. *http://mathworld.wolfram.com/MaximumLikelihood.html* (March 27 2015).

[25] Wit, E., van den Heuvel, E., and Romeijn, J.-W. 'all models are wrong...': an introduction to model uncertainty. *Statistica Neerlandica 66*, 3 (2012), 217–236.

[26] Woodhouse, J. H., Giardini, D., and Li, X.-D. Evidence for inner core anisotropy from free oscillations. *Geophysical Research Letters 13*, 13 (December 1986), 1549–1552.

Appendix A

Seismic wave phases

A standard seismic phase listing was created by an International Association of Seismology and Physics of the Earth's Interior (IASPEI) working group that was created in 2001 and ratified in 2003 [4]. Below is a partial listing of seismic phase nomenclature that is important when studying the inner core of the Earth. Upper case denotes a refracted wave, and lower case denotes a reflected wave.[1]

- P – longitudinal (P) wave that has travelled through Earth's crust and mantle
- K – longitudinal (P) wave that has travelled through Earth's outer core
- I – longitudinal (P) wave that has travelled through Earth's inner core
- S – transverse (S) wave that has travelled through Earth's crust and mantle
- J – transverse (S) wave that has travelled through Earth's inner core
- i – longitudinal (P) wave that has reflected off Earth's inner core - outer core boundary

There are many waves for studying the inner core, two of the simplest waves to observe are the PKIKP wave and the PKiKP wave. The PKIKP wave is a

[1]For a full listing of seismic wave phases see The IASPEI Standard Seismic Phase List [4]

wave that has traveled through the crust and mantle, then the outer core, then the inner core, then the outer core again and through the mantle and crust again. The PKiKP wave, read left to right, travels initially through the crust and mantle, then the outer core, then reflects off the inner core - outer core boundary, travels back through the outer core, and then though the mantle and crust again.

Appendix B

Kolmogorov-Smirnov Test

The Kolmogorov-Smirnov (KS) test is a nonparametric statistical test that can be used to measure the similarity between datasets. It is a goodness-of-fit test that can be used for any statistical distribution. It can be used to test for the distribution of a dataset, or test the similarity between two datasets.

To use the KS test to test the similarity between datasets, the cumulative distribution functions for both datasets need to be computed, and the maximum difference between them needs to be calculated, namely,

$$d = \sup_x |F_{1,n}(x) - F_{2,n}(x)| \,,$$

where, $F_{\cdot,n}(x)$, is the cumulative distribution function, and sup is the supremum function. The D-Statistic then needs to be calculated. The D-Statistic is based on the number of samples being compared,

$$D_n = 1.36\sqrt{\frac{n_1 + n_2}{(n_1 n_2)}} \,,$$

where D_n is the D-Statistic, n_1 is the the number of data points in data set one, and n_2 is the number of data points in data set two. If d is less than the D-statistic the null-hypothesis that the data comes from the same population is rejected [7].

A p-value is often calculated with the KS test as another means of testing the null hypothesis. The p-value is the probability of observing the d value or a d value with even greater evidence against the null hypothesis, even if the null hypothesis is true [14],

$$p = Pr(D_n \leq d).$$

A p-value of 5% is often used as the threshold for rejection of the null hypothesis; however, this is an arbitrary cut off, and other thresholds can be used. A p-value threshold of 5% means that based on the data available to the KS test, we reject the null hypothesis that the data comes from the same population if there is a 5% or less probability of a greater variance in data being due to random errors in the data.

Appendix C

Central Limit Theorem

The Central Limit Theorem was proposed by Abraham de Moivre, a French mathematician who in 1733 published an article using normal distribution to approximate the number of "heads" resulting from tosses of a fair coin. It was later rediscovered by Pierre-Simon Laplace and published in his 1812 work *Théorie Analytique des Probabilités*. It was not until the turn of the 20th century that the Central Limit Theorem took the form that we know today as generalized by the Russian mathematician Aleksandr Lyapunov [20].

The theorem states that the sum of a sufficiently large number of independent random variables is approximately normally distributed. Mathematically the theorem for any real numbers a and b is

$$\lim_{n\to\infty} P\left(a \leq \frac{X_1 + X_2 + \cdots + X_n - n\mu}{\sigma\sqrt{n}} \leq b\right) = \Phi(b) - \Phi(a),$$

where $X_1, \ldots, X_n$ is a sequence of independent random variables, $\mu = E(X)$ is the expected value of X, $\sigma = \sigma(X)$ is the standard deviation and $\Phi(x)$ is the standard normal distribution function defined by

$$\Phi(x) = \frac{1}{\sqrt{2\pi}} \int_{-\infty}^{x} e^{\frac{-1}{2}y^2} dy,$$

meaning the standardized variable $(X_1 + X_2 + \cdots + X_n - n\mu)/\sigma\sqrt{n}$ is approximately normally distributed [20].

Appendix D

Bayesian Information Criterion

Choosing an appropriate model to represent a set of data can be a very difficult task. Models with more parameters fit measurements better than models with fewer parameters; however, in accordance with the concept of Occam's Razor, we must pick the simplest model to represent our data. BIC can be used for model selection amongst a finite set of models; it provides a way to test if there is justification for choosing a more complicated model over a simpler model.

BIC is a modification of the Akaike Information Criterion (AIC) that was proposed by Gideon Schwarz in the 1978 paper *Estimating the dimension of a model* in which he provided a Bayesian argument for its adoption [16]. The BIC of a model can be expressed as

$$BIC = -2\ln(L) + k\ln(n),$$

where L is the maximum likelihood function for the model, n is the number of data points and k is the number of free parameters to be estimated [25]. The maximum likelihood in the case of a function that is normally distributed is [24]

$$L = \frac{(2\pi)^{-n/2}}{\sigma^n} \exp\left[-\frac{\sum(x_i - \mu)^2}{2\sigma^2} \right],$$

where

$$\mu = \frac{\sum x_i}{n}$$

and

$$\sigma = \sqrt{\frac{\sum (x_i - \mu)^2}{n}}.$$

The model with the lowest BIC is considered the most appropriate model given the information available. Compared with the AIC,

$$AIC = -2\ln(L) + 2k\,,$$

For $n > 8$ the BIC penalty, $k\ln(n)$, is greater than the AIC penalty, $2k$. Therefore, relative to AIC, BIC tends to favour simpler models, that is, models with fewer parameters. [12].

Appendix E

Preliminary Reference Earth Model

PREM was created by Dziewonski and Anderson in 1981 [9] as a reference model of the Earth, representative of both body waves and normal mode observations. PREM was created using three subsets of data: *Astronomic-geodetic data*, *Free oscillation and long-period surface wave data*, and *Body-wave data*. These three subsets made up an extremely large data set encompassing about 1000 normal mode periods, 500 summary traveltime observations,100 normal mode seismic quality factor (Q) values, and 12 years of International Seismological Centre (ISC) observations totalling 1.75×10^6 P and S wave traveltime observations. Q values and density of the Earth's interior were obtained from mass and moment of inertia inversion.

PREM is a mathematical model of the Earth, meaning that while it does a good job of approximating the structure of the Earth, at no point does the model truly reflect the structure of the Earth; one of the accuracy problems of the model is the extreme anisotropy exhibited in the Earth's crust. In order to account for the anisotropy and inhomogeneity, a weighted average was used to define the upper 100 km of the Earth. Another important assumption made was that Q, which is

the attenuation factor, is independent of frequency.

In PREM, there are nine regions recognized in the Earth's structure:

1. Ocean layer.
2. Upper and lower crust.
3. Region above the low-velocity zone (LID), the main part of the seismic lithosphere.
4. Low velocity zone (LVZ).
5. Region between low velocity zone and 400 km discontinuity.
6. Transition zone spanning the region between 400 and 670 km discontinuities.
7. Lower mantle.
8. Outer core.
9. Inner core.

The subdivision of PREM into nine regions was done to allow a modular construction of the model. Different modules combined to create the whole Earth model allows for changing particular features of a module without having to change all the features in the model. This allows for the creation of a model that has an anisotropic upper mantle, caused mostly by large amounts of anisotropic minerals olivine and pyroxene, while keeping the remaining zones of the Earth model isotropic. PREM values are displayed in tables E.1, and E.2.

Region	Radius (km)	Density (g/cm^3)	V_p (km/s)	V_{avg} (km/s)
Inner Core	0-1221.5	$13.0885 - 8.8381x^2$	$11.2622 - 6.3640x^2$	11.1842
Outer Core	1221.5-3480.0	$12.5815 - 1.2638x - 3.6426x^2 - 5.5281x^3$	$11.0487 - 4.0362x + 4.8023x^2 - 13.5732x^3$	9.2993
Lower Mantle	3480.0-3630.0	$7.9565 - 6.4761x + 5.5283x^2 - 3.0807x^3$	$15.3891 - 5.3181x + 5.5242x^2 - 2.5514x^3$	13.6984
	3630.0-5600.0	$7.9565 - 6.4761x + 5.5283x^2 - 3.0807x^3$	$24.9520 - 40.4673x + 51.4832x^2 - 26.6419x^3$	12.4752
	5600.0-5701.0	$7.9565 - 6.4761x + 5.5283x^2 - 3.0807x^3$	$29.2766 - 23.6027x + 5.5242x^2 - 2.5514x^3$	10.9085
Transition zone	5701.0-5771.0	$5.3197 - 1.4836x$	$19.0957 - 9.8672x$	10.2120
	5771.0-5971.0	$11.2494 - 8.0298x$	$39.7027 - 32.6166x$	
	5971.0-6151.0	$7.1089 - 3.8045x$	$20.3926 - 12.2569x$	9.6464

Table E.1: PREM model values of density and P wave velocities up to transversely isotopic region; average velocities calculated using expression (4.1). The variable x is the normalized radius, where $x = r/a$, r is the radius, and $a = 6371$km.

LVZ	6151.0-6291.0	2.2910 $+0.6924x$	V_{PV} 0.8317 $+7.2180x$ V_{PH} 3.5908 $+4.6172x$	
LID	6291.0-6346.6	2.6910 $+0.6924x$	V_{PV} 0.8317 $+7.2180x$ V_{PH} 3.5908 $+4.6172x$	
Crust	6346.6-6356.0	2.900	6.800	6.800
Ocean	6368.0-6371.0	1.020	1.450	1.450
Iso approx. Ocean-LVZ			4.1875 $+3.9382x$	

Table E.2: Transversely isotropic region of PREM model and isotropic approximation

Appendix F

Mathematica Code

The Mathematica code included was used to generate Model 1. Changing the source location, the receivers being used, the errors introduced into the forward model, and the number of traveltime measurements modifies the code for models 2 and 3. This code could also be easily modified to be representative of a VSP by changing the velocity properties, along with sources and receivers.

Code

```
Remove["Global*"]
```

Set Source and Receiver locations at positions measured from vertical axis.

Calculate ray angle and distance between source and receivers

```
Sx:=N[1200Cos[Degree90]]
Sy:=N[1200Sin[Degree90]]
S:={Sx, Sy}
R1x:=N[1200Cos[Degree100]];
R1y:=N[1200Sin[100π/180]];
```

$$D1:=\sqrt{(Sx-R1x)^2+(Sy-R1y)^2};$$

$$A1:=Abs[Sy-R1y]$$

$$th1:=ArcCos[A1/D1]$$

$$R1:=\{R1x,R1y\}$$

$$R2x:=N[1200Cos[110\pi/180]];$$

$$R2y:=N[1200Sin[110\pi/180]];$$

$$D2:=\sqrt{(Sx-R2x)^2+(Sy-R2y)^2};$$

$$A2:=Abs[Sy-R2y]$$

$$th2:=ArcCos[A2/D2];$$

$$R2:=\{R2x,R2y\};$$

$$R3x:=N[1200Cos[120\pi/180]];$$

$$R3y:=N[1200Sin[120\pi/180]];$$

$$D3:=\sqrt{(Sx-R3x)^2+(Sy-R3y)^2};$$

$$A3:=Abs[Sy-R3y]$$

$$th3:=ArcCos[A3/D3];$$

$$R3:=\{R3x,R3y\};$$

$$R4x:=N[1200Cos[130\pi/180]];$$

$$R4y:=N[1200Sin[130\pi/180]];$$

$$D4:=\sqrt{(Sx-R4x)^2+(Sy-R4y)^2};$$

$$A4:=Abs[Sy-R4y]$$

$$th4:=ArcCos[A4/D4];$$

$$R4:=\{R4x,R4y\};$$

$$R5x:=N[1200Cos[140\pi/180]];$$

$$R5y:=N[1200Sin[140\pi/180]];$$

$$D5:=\sqrt{(Sx-R5x)^2+(Sy-R5y)^2};$$

$$R5:=\{R5x,R5y\};$$

$$A5:=Abs[Sy-R5y]$$

$$th5:=ArcCos[A5/D5];$$

R6x:=N[1200Cos[150π/180]];

R6y:=N[1200Sin[150π/180]];

D6:=$\sqrt{(Sx - R6x)^2 + (Sy - R6y)^2}$;

R6:={R6x, R6y};

A6:=Abs[Sy − R6y]

th6:=ArcCos[A6/D6];

R7x:=N[1200Cos[160π/180]];

R7y:=N[1200Sin[160π/180]];

D7:=$\sqrt{(Sx - R7x)^2 + (Sy - R7y)^2}$;

R7:={R7x, R7y};

A7:=Abs[Sy − R7y]

th7:=ArcCos[A7/D7];

R8x:=N[1200Cos[170π/180]];

R8y:=N[1200Sin[170π/180]];

D8:=$\sqrt{(Sx - R8x)^2 + (Sy - R8y)^2}$;

R8:={R8x, R8y};

A8:=Abs[Sy − R8y]

th8:=ArcCos[A8/D8];

R9x:=N[1200Cos[180π/180]];

R9y:=N[1200Sin[180π/180]];

D9:=$\sqrt{(Sx - R9x)^2 + (Sy - R9y)^2}$;

R9:={R9x, R9y};

A9:=Abs[Sy − R9y]

th9:=ArcCos[A9/D9];

R10x:=N[1200Cos[190π/180]];

R10y:=N[1200Sin[190π/180]];

D10:=$\sqrt{(Sx - R10x)^2 + (Sy - R10y)^2}$;

R10:={R10x, R10y};

A10:=Abs[Sy − R10y]

th10:=ArcCos[A10/D10];

R11x:=N[1200Cos[200π/180]];

R11y:=N[1200Sin[200π/180]];

D11:=$\sqrt{(\mathrm{Sx} - \mathrm{R11x})^2 + (\mathrm{Sy} - \mathrm{R11y})^2}$;

R11:={R11x, R11y};

A11:=Abs[Sy − R11y]

th11:=ArcCos[A11/D11]

R12x:=N[1200Cos[210π/180]];

R12y:=N[1200Sin[210π/180]];

D12:=$\sqrt{(\mathrm{Sx} - \mathrm{R12x})^2 + (\mathrm{Sy} - \mathrm{R12y})^2}$;

R12:={R12x, R12y};

A12:=Abs[Sy − R12y]

th12:=ArcCos[A12/D12];

R13x:=N[1200Cos[220π/180]];

R13y:=N[1200Sin[220π/180]];

D13:=$\sqrt{(\mathrm{Sx} - \mathrm{R13x})^2 + (\mathrm{Sy} - \mathrm{R13y})^2}$;

R13:={R13x, R13y};

A13:=Abs[Sy − R13y]

th13:=ArcCos[A13/D13];

R14x:=N[1200Cos[230π/180]];

R14y:=N[1200Sin[230π/180]];

D14:=$\sqrt{(\mathrm{Sx} - \mathrm{R14x})^2 + (\mathrm{Sy} - \mathrm{R14y})^2}$;

R14:={R14x, R14y};

A14 = Abs[Sy − R14y]

th14:=ArcCos[A14/D14];

2119.25

R15x:=N[1200Cos[240π/180]];

R15y:=N[1200Sin[240π/180]];

D15:=$\sqrt{(\text{Sx}-\text{R15x})^2+(\text{Sy}-\text{R15y})^2}$;

R15:={R15x, R15y};

A15:=Abs[Sy − R15y]

th15:=ArcCos[A15/D15];

R16x:=N[1200Cos[250π/180]];

R16y:=N[1200Sin[250π/180]];

D16:=$\sqrt{(\text{Sx}-\text{R16x})^2+(\text{Sy}-\text{R16y})^2}$;

R16:={R16x, R16y};

A16:=Abs[Sy − R16y]

th16:=ArcCos[A16/D16];

R17x:=N[1200Cos[260π/180]];

R17y:=N[1200Sin[260π/180]];

D17:=$\sqrt{(\text{Sx}-\text{R17x})^2+(\text{Sy}-\text{R17y})^2}$;

R17:={R17x, R17y};

A17:=Abs[Sy − R17y]

th17:=ArcCos[A17/D17];

R18x:=N[1200Cos[270π/180]];

R18y:=N[1200Sin[270π/180]];

D18:=$\sqrt{(\text{Sx}-\text{R18x})^2+(\text{Sy}-\text{R18y})^2}$;

R18:={R18x, R18y};

A18:=Abs[Sy − R18y]

th18:=ArcCos[A18/D18];

Plot source and receivers to insure no errors in locations

ListPlot[{S, R1, R2, R3, R4, R5, R6, R7, R8, R9, R10, R11, R12, R13, R14, R15, R16, R17, R18},
AspectRatio → 1, PlotRange → {{1300, −1300}, {1300, −1300}}, AxesOrigin → {0, 0}]

Calculate Elliptical Velocity

$$V[\theta\_]:=\text{Vz}\sqrt{\frac{(1+(\text{Tan}[\theta])^2)}{1+\left(\frac{\text{Vz}}{\text{Vx}}\right)^2(\text{Tan}[\theta])^2}}$$

$$\text{Vx}:=11.2$$

$$\text{Vz}:=11.2+11.2(0.05)$$

Velocity for each ray angle calculated

$$\text{V1}:=V[\text{th1}];$$

$$\text{V2}:=V[\text{th2}];$$

$$\text{V3}:=V[\text{th3}];$$

$$\text{V4}:=V[\text{th4}];$$

$$\text{V5}:=V[\text{th5}];$$

$$\text{V6}:=V[\text{th6}];$$

$$\text{V7}:=V[\text{th7}];$$

$$\text{V8}:=V[\text{th8}];$$

$$\text{V9}:=V[\text{th9}];$$

$$\text{V10}:=V[\text{th10}];$$

$$\text{V11}:=V[\text{th11}];$$

$$\text{V12}:=V[\text{th12}];$$

$$\text{V13}:=V[\text{th13}];$$

$$\text{V14}:=V[\text{th14}];$$

$$\text{V15}:=V[\text{th15}];$$

$$\text{V16}:=V[\text{th16}];$$

$$\text{V17}:=V[\text{th17}];$$

$$\text{V18}:=V[\text{th18}];$$

Elliptical traveltimes

traveltime function with random errors

t1[i_]:=D1/V1 + (D1/V1) * RandomReal[{−0.01, 0.01}];

t2[i_]:=D2/V2 + (D2/V2) * RandomReal[{−0.01, 0.01}];

t3[i_]:=D3/V3 + (D3/V3) * RandomReal[{−0.01, 0.01}];

t4[i_]:=D4/V4 + (D4/V4) * RandomReal[{−0.01, 0.01}];

t5[i_]:=D5/V5 + (D5/V5) * RandomReal[{−0.01, 0.01}];

t6[i_]:=D6/V6 + (D6/V6) * RandomReal[{−0.01, 0.01}];

t7[i_]:=D7/V7 + (D7/V7) * RandomReal[{−0.01, 0.01}];

t8[i_]:=D8/V8 + (D8/V8) * RandomReal[{−0.01, 0.01}];

t9[i_]:=D9/V9 + (D9/V9) * RandomReal[{−0.01, 0.01}];

t10[i_]:=D10/V10 + (D10/V10) * RandomReal[{−0.01, 0.01}];

t11[i_]:=D11/V11 + (D11/V11) * RandomReal[{−0.01, 0.01}];

t12[i_]:=D12/V12 + (D12/V12) * RandomReal[{−0.01, 0.01}];

t13[i_]:=D13/V13 + (D13/V13) * RandomReal[{−0.01, 0.01}];

t14[i_]:=D14/V14 + (D14/V14) * RandomReal[{−0.01, 0.01}];

t15[i_]:=D15/V15 + (D15/V15) * RandomReal[{−0.01, 0.01}];

t16[i_]:=D16/V16 + (D16/V16) * RandomReal[{−0.01, 0.01}];

t17[i_]:=D17/V17 + (D17/V17) * RandomReal[{−0.01, 0.01}];

t18[i_]:=D18/V18 + (D18/V18) * RandomReal[{−0.01, 0.01}];

Calculate 10 traveltimes at each receiver location and export calculated traveltimes to save data

tell1:=Table[t1[i_], {i, 10}]

tell2:=Table[t2[i_], {i, 10}]

tell3:=Table[t3[i_], {i, 10}]

tell4:=Table[t4[i_], {i, 10}]

tell5:=Table[t5[i_], {i, 10}]

tell6:=Table[t6[i_], {i, 10}]

tell7:=Table[t7[i_], {i, 10}]

tell8:=Table[t8[i_], {i, 10}]

tell9:=Table[t9[i_], {i, 10}]

tell10:=Table[t10[i_], {i, 10}]

tell11:=Table[t11[i_], {i, 10}]

tell12:=Table[t12[i_], {i, 10}]

tell13:=Table[t13[i_], {i, 10}]

tell14:=Table[t14[i_], {i, 10}]

tell15:=Table[t15[i_], {i, 10}]

tell16:=Table[t16[i_], {i, 10}]

tell17:=Table[t17[i_], {i, 10}]

tell18:=Table[t18[i_], {i, 10}]

Export["Filelocation/filename.dat", tell1];

Import traveltimes for each receiver using following scheme

te1:=Flatten[Import["Filelocation/filename.dat"]]

Calculate average traveltime for each receiver

tm1 = Mean[te1];

tm2 = Mean[te2];

tm3 = Mean[te3];

tm4 = Mean[te4];

tm5 = Mean[te5];

tm6 = Mean[te6];

tm7 = Mean[te7];

tm8 = Mean[te8];

tm9 = Mean[te9];

tm10 = Mean[te10];

tm11 = Mean[te11];

tm12 = Mean[te12];

tm13 = Mean[te13];

tm14 = Mean[te14];

tm15 = Mean[te15];

tm16 = Mean[te16];

tm17 = Mean[te17];

tm18 = Mean[te18];

Calculate error to be introduced into isotropic traveltimes

er1:=3(StandardDeviation[te1])/Mean[te1]

er2:=3(StandardDeviation[te2])/Mean[te2]

er3:=3(StandardDeviation[te3])/Mean[te3]

er4:=3(StandardDeviation[te4])/Mean[te4]

er5:=3(StandardDeviation[te5])/Mean[te5]

er6:=3(StandardDeviation[te6])/Mean[te6]

er7:=3(StandardDeviation[te7])/Mean[te7]

er8:=3(StandardDeviation[te8])/Mean[te8]

er9:=3(StandardDeviation[te9])/Mean[te9]

er10:=3(StandardDeviation[te10])/Mean[te10]

er11:=3(StandardDeviation[te11])/Mean[te11]

er12:=3(StandardDeviation[te12])/Mean[te12]

er13:=3(StandardDeviation[te13])/Mean[te13]

er14:=3(StandardDeviation[te14])/Mean[te14]

er15:=3(StandardDeviation[te15])/Mean[te15]

er16:=3(StandardDeviation[te16])/Mean[te16]

er17:=3(StandardDeviation[te17])/Mean[te17]

er18:=3(StandardDeviation[te18])/Mean[te18]

Elliptical minimization function

$$\text{STISO}[vx\_, vz\_] := \text{Abs}\left[\text{tm1} - \frac{\text{D1}}{\text{vz}\sqrt{\frac{(1+(\text{Tan}[\text{th1}])^2)}{1+(\frac{\text{vz}}{\text{vx}})^2(\text{Tan}[\text{th1}])^2}}}\right] + \text{Abs}\left[\text{tm2} - \frac{\text{D2}}{\text{vz}\sqrt{\frac{(1+(\text{Tan}[\text{th2}])^2)}{1+(\frac{\text{vz}}{\text{vx}})^2(\text{Tan}[\text{th2}])^2}}}\right] +$$
$$\text{Abs}\left[\text{tm3} - \frac{\text{D3}}{\text{vz}\sqrt{\frac{(1+(\text{Tan}[\text{th3}])^2)}{1+(\frac{\text{vz}}{\text{vx}})^2(\text{Tan}[\text{th3}])^2}}}\right] + \text{Abs}\left[\text{tm4} - \frac{\text{D4}}{\text{vz}\sqrt{\frac{(1+(\text{Tan}[\text{th4}])^2)}{1+(\frac{\text{vz}}{\text{vx}})^2(\text{Tan}[\text{th4}])^2}}}\right] +$$
$$\text{Abs}\left[\text{tm5} - \frac{\text{D5}}{\text{vz}\sqrt{\frac{(1+(\text{Tan}[\text{th5}])^2)}{1+(\frac{\text{vz}}{\text{vx}})^2(\text{Tan}[\text{th5}])^2}}}\right] + \text{Abs}\left[\text{tm6} - \frac{\text{D6}}{\text{vz}\sqrt{\frac{(1+(\text{Tan}[\text{th6}])^2)}{1+(\frac{\text{vz}}{\text{vx}})^2(\text{Tan}[\text{th6}])^2}}}\right] +$$
$$\text{Abs}\left[\text{tm7} - \frac{\text{D7}}{\text{vz}\sqrt{\frac{(1+(\text{Tan}[\text{th7}])^2)}{1+(\frac{\text{vz}}{\text{vx}})^2(\text{Tan}[\text{th7}])^2}}}\right] + \text{Abs}\left[\text{tm8} - \frac{\text{D8}}{\text{vz}\sqrt{\frac{(1+(\text{Tan}[\text{th8}])^2)}{1+(\frac{\text{vz}}{\text{vx}})^2(\text{Tan}[\text{th8}])^2}}}\right] +$$
$$\text{Abs}\left[\text{tm9} - \frac{\text{D9}}{\text{vz}\sqrt{\frac{(1+(\text{Tan}[\text{th9}])^2)}{1+(\frac{\text{vz}}{\text{vx}})^2(\text{Tan}[\text{th9}])^2}}}\right] + \text{Abs}\left[\text{tm10} - \frac{\text{D10}}{\text{vz}\sqrt{\frac{(1+(\text{Tan}[\text{th10}])^2)}{1+(\frac{\text{vz}}{\text{vx}})^2(\text{Tan}[\text{th10}])^2}}}\right] +$$
$$\text{Abs}\left[\text{tm11} - \frac{\text{D11}}{\text{vz}\sqrt{\frac{(1+(\text{Tan}[\text{th11}])^2)}{1+(\frac{\text{vz}}{\text{vx}})^2(\text{Tan}[\text{th11}])^2}}}\right] + \text{Abs}\left[\text{tm12} - \frac{\text{D12}}{\text{vz}\sqrt{\frac{(1+(\text{Tan}[\text{th12}])^2)}{1+(\frac{\text{vz}}{\text{vx}})^2(\text{Tan}[\text{th12}])^2}}}\right] +$$
$$\text{Abs}\left[\text{tm13} - \frac{\text{D13}}{\text{vz}\sqrt{\frac{(1+(\text{Tan}[\text{th13}])^2)}{1+(\frac{\text{vz}}{\text{vx}})^2(\text{Tan}[\text{th13}])^2}}}\right] + \text{Abs}\left[\text{tm14} - \frac{\text{D14}}{\text{vz}\sqrt{\frac{(1+(\text{Tan}[\text{th14}])^2)}{1+(\frac{\text{vz}}{\text{vx}})^2(\text{Tan}[\text{th14}])^2}}}\right] +$$
$$\text{Abs}\left[\text{tm15} - \frac{\text{D15}}{\text{vz}\sqrt{\frac{(1+(\text{Tan}[\text{th15}])^2)}{1+(\frac{\text{vz}}{\text{vx}})^2(\text{Tan}[\text{th15}])^2}}}\right] + \text{Abs}\left[\text{tm16} - \frac{\text{D16}}{\text{vz}\sqrt{\frac{(1+(\text{Tan}[\text{th16}])^2)}{1+(\frac{\text{vz}}{\text{vx}})^2(\text{Tan}[\text{th16}])^2}}}\right] +$$

$$\text{Abs}\left[\text{tm17} - \frac{\text{D17}}{\text{vz}\sqrt{\frac{(1+(\text{Tan[th17]})^2)}{1+(\frac{\text{vz}}{\text{vx}})^2(\text{Tan[th17]})^2}}}\right] + \text{Abs}\left[\text{tm18} - \frac{\text{D18}}{\text{vz}\sqrt{\frac{(1+(\text{Tan[th18]})^2)}{1+(\frac{\text{vz}}{\text{vx}})^2(\text{Tan[th18]})^2}}}\right]$$

$$\text{STI} = \text{NMinimize}[\text{STISO}[\text{vx}, \text{vz}], \{\text{vx} < \text{vz}, 13 > \text{vz} > 10.5\}, \{\text{vx}, \text{vz}\}, \text{MaxIterations} \to 1000]$$

$$\{3.55361, \{\text{vx} \to 11.2075, \text{vz} \to 11.7556\}\}$$

Isotropic velocity minimization function

$$\text{SX[v\_]:=Abs}\left[\text{tm1} - \frac{\text{D1}}{v}\right] + \text{Abs}\left[\text{tm2} - \frac{\text{D2}}{v}\right] + \text{Abs}\left[\text{tm3} - \frac{\text{D3}}{v}\right] + \text{Abs}\left[\text{tm4} - \frac{\text{D4}}{v}\right] + \text{Abs}\left[\text{tm5} - \frac{\text{D}}{}\right.$$

$$\text{Abs}\left[\text{tm6} - \frac{\text{D6}}{v}\right] + \text{Abs}\left[\text{tm7} - \frac{\text{D7}}{v}\right] + \text{Abs}\left[\text{tm8} - \frac{\text{D8}}{v}\right] + \text{Abs}\left[\text{tm9} - \frac{\text{D9}}{v}\right] + \text{Abs}\left[\text{tm10} - \frac{\text{D10}}{v}\right] +$$

$$\text{Abs}\left[\text{tm11} - \frac{\text{D11}}{v}\right] + \text{Abs}\left[\text{tm12} - \frac{\text{D12}}{v}\right] + \text{Abs}\left[\text{tm13} - \frac{\text{D13}}{v}\right] + \text{Abs}\left[\text{tm14} - \frac{\text{D14}}{v}\right] + \text{Abs}\left[\text{tm15} - \frac{\text{D}}{}\right.$$

$$\text{Abs}\left[\text{tm16} - \frac{\text{D16}}{v}\right] + \text{Abs}\left[\text{tm17} - \frac{\text{D17}}{v}\right] + \text{Abs}\left[\text{tm18} - \frac{\text{D18}}{v}\right]$$

$$\text{SISO} = \text{Minimize}[\text{SX}[v], v]$$

$$\{29.4111, \{v \to 11.6348\}\}$$

Isotraveltimes

Input isotropic velocity from minimization

Viso : 11.639842723949194

Create isotropic traveltime function with calculated isotropic velocity and errors

$$\text{i1[i\_]:=D1/Viso} + (\text{D1/Viso}) * \text{RandomReal}[\{-\text{er1}, \text{er1}\}];$$

$$\text{i2[i\_]:=D2/Viso} + (\text{D2/Viso}) * \text{RandomReal}[\{-\text{er2}, \text{er2}\}];$$

$$\text{i3[i\_]:=D3/Viso} + (\text{D3/Viso}) * \text{RandomReal}[\{-\text{er3}, \text{er3}\}];$$

```
i4[i_]:=D4/Viso + (D4/Viso) * RandomReal[{-er4, er4}];
i5[i_]:=D5/Viso + (D5/Viso) * RandomReal[{-er5, er5}];
i6[i_]:=D6/Viso + (D6/Viso) * RandomReal[{-er6, er6}];
i7[i_]:=D7/Viso + (D7/Viso) * RandomReal[{-er7, er7}];
i8[i_]:=D8/Viso + (D8/Viso) * RandomReal[{-er8, er8}];
i9[i_]:=D9/Viso + (D9/Viso) * RandomReal[{-er9, er9}];
i10[i_]:=D10/Viso + (D10/Viso) * RandomReal[{-er10, er10}];
i11[i_]:=D11/Viso + (D11/Viso) * RandomReal[{-er11, er11}];
i12[i_]:=D12/Viso + (D12/Viso) * RandomReal[{-er12, er12}];
i13[i_]:=D13/Viso + (D13/Viso) * RandomReal[{-er13, er13}];
i14[i_]:=D14/Viso + (D14/Viso) * RandomReal[{-er14, er14}];
i15[i_]:=D15/Viso + (D15/Viso) * RandomReal[{-er15, er15}];
i16[i_]:=D16/Viso + (D16/Viso) * RandomReal[{-er16, er16}];
i17[i_]:=D17/Viso + (D17/Viso) * RandomReal[{-er17, er17}];
i18[i_]:=D18/Viso + (D18/Viso) * RandomReal[{-er18, er18}];
```

Calculate 10 traveltimes for each receiver location

```
tiso1:=Table[i1[i_], {i, 10}]
tiso2:=Table[i2[i_], {i, 10}]
tiso3:=Table[i3[i_], {i, 10}]
tiso4:=Table[i4[i_], {i, 10}]
tiso5:=Table[i5[i_], {i, 10}]
tiso6:=Table[i6[i_], {i, 10}]
tiso7:=Table[i7[i_], {i, 10}]
tiso8:=Table[i8[i_], {i, 10}]
tiso9:=Table[i9[i_], {i, 10}]
tiso10:=Table[i10[i_], {i, 10}]
```

tiso11:=Table[i11[i_], {i, 10}]

tiso12:=Table[i12[i_], {i, 10}]

tiso13:=Table[i13[i_], {i, 10}]

tiso14:=Table[i14[i_], {i, 10}]

tiso15:=Table[i15[i_], {i, 10}]

tiso16:=Table[i16[i_], {i, 10}]

tiso17:=Table[i17[i_], {i, 10}]

tiso18:=Table[i18[i_], {i, 10}]

Export isotropic traveltimes to save values using following template for each receiver

Export["Filelocation/filename.dat", tiso1];

Import isotropic traveltimes for each receiver using following scheme

ti1:=Flatten[Import["Filelocation/filename.dat"]]

KS Test

KolmogorovSmirnovTest[ti1, te1, "TestDataTable"]

	Statistic	P-Value
Kolmogorov-Smirnov	1.	0.0000108251

KolmogorovSmirnovTest[ti2, te2, "TestDataTable"]

	Statistic	P-Value
Kolmogorov-Smirnov	1.	0.0000108251

KolmogorovSmirnovTest[ti3, te3, "TestDataTable"]

	Statistic	P-Value
Kolmogorov-Smirnov	1.	0.0000108251

KolmogorovSmirnovTest[ti4, te4, "TestDataTable"]

	Statistic	P-Value
Kolmogorov-Smirnov	1.	0.0000108251

KolmogorovSmirnovTest[ti5, te5, "TestDataTable"]

	Statistic	P-Value
Kolmogorov-Smirnov	1.	0.0000108251

KolmogorovSmirnovTest[ti6, te6, "TestDataTable"]

	Statistic	P-Value
Kolmogorov-Smirnov	1.	0.0000108251

KolmogorovSmirnovTest[ti7, te7, "TestDataTable"]

	Statistic	P-Value
Kolmogorov-Smirnov	1.	0.0000108251

KolmogorovSmirnovTest[ti8, te8, "TestDataTable"]

	Statistic	P-Value
Kolmogorov-Smirnov	1.	0.0000108251

KolmogorovSmirnovTest[ti9, te9, "TestDataTable"]

	Statistic	P-Value
Kolmogorov-Smirnov	1.	0.0000108251

KolmogorovSmirnovTest[ti10, te10, "TestDataTable"]

	Statistic	P-Value
Kolmogorov-Smirnov	0.9	0.000216502

KolmogorovSmirnovTest[ti11, te11, "TestDataTable"]

	Statistic	P-Value
Kolmogorov-Smirnov	0.8	0.00205677

KolmogorovSmirnovTest[ti12, te12, "TestDataTable"]

	Statistic	P-Value
Kolmogorov-Smirnov	0.7	0.0123406

KolmogorovSmirnovTest[ti13, te13, "TestDataTable"]

	Statistic	P-Value
Kolmogorov-Smirnov	0.5	0.167821

KolmogorovSmirnovTest[ti14, te14, "TestDataTable"]

	Statistic	P-Value
Kolmogorov-Smirnov	0.4	0.417524

KolmogorovSmirnovTest[ti15, te15, "TestDataTable"]

	Statistic	P-Value
Kolmogorov-Smirnov	0.4	0.417524

KolmogorovSmirnovTest[ti16, te16, "TestDataTable"]

	Statistic	P-Value
Kolmogorov-Smirnov	0.4	0.417524

KolmogorovSmirnovTest[ti17, te17, "TestDataTable"]

	Statistic	P-Value
Kolmogorov-Smirnov	0.5	0.167821

KolmogorovSmirnovTest[ti18, te18, "TestDataTable"]

	Statistic	P-Value
Kolmogorov-Smirnov	0.4	0.417524

BIC Input velocities

vzi:=11.755596638891543

vxi:=11.207450704709764

vi:=11.634841192501593

Liklihood calculations

$$\mu\text{TI}:=$$

$$\left(\text{tm1}-\frac{\text{D1}}{\text{vzi}\sqrt{\frac{(1+(\text{Tan[th1]})^2)}{1+\left(\frac{\text{vzi}}{\text{vxi}}\right)^2(\text{Tan[th1]})^2}}}+\text{tm2}-\frac{\text{D2}}{\text{vzi}\sqrt{\frac{(1+(\text{Tan[th2]})^2)}{1+\left(\frac{\text{vzi}}{\text{vxi}}\right)^2(\text{Tan[th2]})^2}}}+\text{tm3}-\frac{\text{D3}}{\text{vzi}\sqrt{\frac{(1+(\text{Tan[th3]})^2)}{1+\left(\frac{\text{vzi}}{\text{vxi}}\right)^2(\text{Tan[th3]})^2}}}+\right.$$

$$\text{tm4}-\frac{\text{D4}}{\text{vzi}\sqrt{\frac{(1+(\text{Tan[th4]})^2)}{1+\left(\frac{\text{vzi}}{\text{vxi}}\right)^2(\text{Tan[th4]})^2}}}+\text{tm5}-\frac{\text{D5}}{\text{vzi}\sqrt{\frac{(1+(\text{Tan[th5]})^2)}{1+\left(\frac{\text{vzi}}{\text{vxi}}\right)^2(\text{Tan[th5]})^2}}}+\text{tm6}-$$

$$\frac{\text{D6}}{\text{vzi}\sqrt{\frac{(1+(\text{Tan[th6]})^2)}{1+\left(\frac{\text{vzi}}{\text{vxi}}\right)^2(\text{Tan[th6]})^2}}}+\text{tm7}-\frac{\text{D7}}{\text{vzi}\sqrt{\frac{(1+(\text{Tan[th7]})^2)}{1+\left(\frac{\text{vzi}}{\text{vxi}}\right)^2(\text{Tan[th7]})^2}}}+\text{tm8}-\frac{\text{D8}}{\text{vzi}\sqrt{\frac{(1+(\text{Tan[th8]})^2)}{1+\left(\frac{\text{vzi}}{\text{vxi}}\right)^2(\text{Tan[th8]})^2}}}+$$

$$\text{tm9}-\frac{\text{D9}}{\text{vzi}\sqrt{\frac{(1+(\text{Tan[th9]})^2)}{1+\left(\frac{\text{vzi}}{\text{vxi}}\right)^2(\text{Tan[th9]})^2}}}+\text{tm10}-\frac{\text{D10}}{\text{vzi}\sqrt{\frac{(1+(\text{Tan[th10]})^2)}{1+\left(\frac{\text{vzi}}{\text{vxi}}\right)^2(\text{Tan[th10]})^2}}}+\text{tm11}-$$

$$\frac{D11}{vzi\sqrt{\frac{(1+(Tan[th11])^2)}{1+\left(\frac{vzi}{vxi}\right)^2(Tan[th11])^2}}}+tm12-\frac{D12}{vzi\sqrt{\frac{(1+(Tan[th12])^2)}{1+\left(\frac{vzi}{vxi}\right)^2(Tan[th12])^2}}}+tm13-$$
$$\frac{D13}{vzi\sqrt{\frac{(1+(Tan[th13])^2)}{1+\left(\frac{vzi}{vxi}\right)^2(Tan[th13])^2}}}+tm14-\frac{D14}{vzi\sqrt{\frac{(1+(Tan[th14])^2)}{1+\left(\frac{vzi}{vxi}\right)^2(Tan[th14])^2}}}+tm15-$$
$$\frac{D15}{vzi\sqrt{\frac{(1+(Tan[th15])^2)}{1+\left(\frac{vzi}{vxi}\right)^2(Tan[th15])^2}}}+tm16-\frac{D16}{vzi\sqrt{\frac{(1+(Tan[th16])^2)}{1+\left(\frac{vzi}{vxi}\right)^2(Tan[th16])^2}}}+tm17-$$
$$\frac{D17}{vzi\sqrt{\frac{(1+(Tan[th17])^2)}{1+\left(\frac{vzi}{vxi}\right)^2(Tan[th17])^2}}}+tm18-\frac{D18}{vzi\sqrt{\frac{(1+(Tan[th18])^2)}{1+\left(\frac{vzi}{vxi}\right)^2(Tan[th18])^2}}}\Bigg)\Big/18$$

$$zTI:=\left(tm1-\frac{D1}{vzi\sqrt{\frac{(1+(Tan[th1])^2)}{1+\left(\frac{vzi}{vxi}\right)^2(Tan[th1])^2}}}-\mu TI\right)^2+\left(tm2-\frac{D2}{vzi\sqrt{\frac{(1+(Tan[th2])^2)}{1+\left(\frac{vzi}{vxi}\right)^2(Tan[th2])^2}}}-\mu TI\right)^2+$$
$$\left(tm3-\frac{D3}{vzi\sqrt{\frac{(1+(Tan[th3])^2)}{1+\left(\frac{vzi}{vxi}\right)^2(Tan[th3])^2}}}-\mu TI\right)^2+\left(tm4-\frac{D4}{vzi\sqrt{\frac{(1+(Tan[th4])^2)}{1+\left(\frac{vzi}{vxi}\right)^2(Tan[th4])^2}}}-\mu TI\right)^2+$$
$$\left(tm5-\frac{D5}{vzi\sqrt{\frac{(1+(Tan[th5])^2)}{1+\left(\frac{vzi}{vxi}\right)^2(Tan[th5])^2}}}-\mu TI\right)^2+\left(tm6-\frac{D6}{vzi\sqrt{\frac{(1+(Tan[th6])^2)}{1+\left(\frac{vzi}{vxi}\right)^2(Tan[th6])^2}}}-\mu TI\right)^2+$$
$$\left(tm7-\frac{D7}{vzi\sqrt{\frac{(1+(Tan[th7])^2)}{1+\left(\frac{vzi}{vxi}\right)^2(Tan[th7])^2}}}-\mu TI\right)^2+\left(tm8-\frac{D8}{vzi\sqrt{\frac{(1+(Tan[th8])^2)}{1+\left(\frac{vzi}{vxi}\right)^2(Tan[th8])^2}}}-\mu TI\right)^2+$$
$$\left(tm9-\frac{D9}{vzi\sqrt{\frac{(1+(Tan[th9])^2)}{1+\left(\frac{vzi}{vxi}\right)^2(Tan[th9])^2}}}-\mu TI\right)^2+\left(tm10-\frac{D10}{vzi\sqrt{\frac{(1+(Tan[th10])^2)}{1+\left(\frac{vzi}{vxi}\right)^2(Tan[th10])^2}}}-\mu TI\right)^2+$$
$$\left(tm11-\frac{D11}{vzi\sqrt{\frac{(1+(Tan[th11])^2)}{1+\left(\frac{vzi}{vxi}\right)^2(Tan[th11])^2}}}-\mu TI\right)^2+\left(tm12-\frac{D12}{vzi\sqrt{\frac{(1+(Tan[th12])^2)}{1+\left(\frac{vzi}{vxi}\right)^2(Tan[th12])^2}}}-\mu TI\right)^2+$$
$$\left(tm13-\frac{D13}{vzi\sqrt{\frac{(1+(Tan[th13])^2)}{1+\left(\frac{vzi}{vxi}\right)^2(Tan[th13])^2}}}-\mu TI\right)^2+\left(tm14-\frac{D14}{vzi\sqrt{\frac{(1+(Tan[th14])^2)}{1+\left(\frac{vzi}{vxi}\right)^2(Tan[th14])^2}}}-\mu TI\right)^2+$$
$$\left(tm15-\frac{D15}{vzi\sqrt{\frac{(1+(Tan[th15])^2)}{1+\left(\frac{vzi}{vxi}\right)^2(Tan[th15])^2}}}-\mu TI\right)^2+\left(tm16-\frac{D16}{vzi\sqrt{\frac{(1+(Tan[th16])^2)}{1+\left(\frac{vzi}{vxi}\right)^2(Tan[th16])^2}}}-\mu TI\right)^2+$$
$$\left(tm17-\frac{D17}{vzi\sqrt{\frac{(1+(Tan[th17])^2)}{1+\left(\frac{vzi}{vxi}\right)^2(Tan[th17])^2}}}-\mu TI\right)^2+\left(tm18-\frac{D18}{vzi\sqrt{\frac{(1+(Tan[th18])^2)}{1+\left(\frac{vzi}{vxi}\right)^2(Tan[th18])^2}}}-\mu TI\right)^2$$
$$\sigma TI:=\sqrt{(zTI)}/18$$

$$\text{liTI}:=\frac{(2\pi)^{-18/2}}{\sigma\text{TI}^{18}}e^{-\text{zTI}/2\sigma\text{TI}^2}$$

$$\mu\text{I}:=$$

$$\left(\text{tm1}-\frac{\text{D1}}{\text{vi}}+\text{tm2}-\frac{\text{D2}}{\text{vi}}+\text{tm3}-\frac{\text{D3}}{\text{vi}}+\text{tm4}-\frac{\text{D4}}{\text{vi}}+\text{tm5}-\frac{\text{D5}}{\text{vi}}+\text{tm6}-\frac{\text{D6}}{\text{vi}}+\text{tm7}-\frac{\text{D7}}{\text{vi}}+\text{tm8}-\frac{\text{D8}}{\text{vi}}\right.$$

$$\text{tm9}-\frac{\text{D9}}{\text{vi}}+\text{tm10}-\frac{\text{D10}}{\text{vi}}+\text{tm11}-\frac{\text{D11}}{\text{vi}}+\text{tm12}-\frac{\text{D12}}{\text{vi}}+\text{tm13}-\frac{\text{D13}}{\text{vi}}+\text{tm14}-\frac{\text{D14}}{\text{vi}}+\text{tm15}-$$

$$\left.\frac{\text{D15}}{\text{vi}}+\text{tm16}-\frac{\text{D16}}{\text{vi}}+\text{tm17}-\frac{\text{D17}}{\text{vi}}+\text{tm18}-\frac{\text{D18}}{\text{vi}}\right)/18$$

$$\text{zI}:=\left(\text{tm1}-\frac{\text{D1}}{\text{vi}}-\mu\text{I}\right)^2+\left(\text{tm2}-\frac{\text{D2}}{\text{vi}}-\mu\text{I}\right)^2+\left(\text{tm3}-\frac{\text{D3}}{\text{vi}}-\mu\text{I}\right)^2+\left(\text{tm4}-\frac{\text{D4}}{\text{vi}}-\mu\text{I}\right)^2+$$

$$\left(\text{tm5}-\frac{\text{D5}}{\text{vi}}-\mu\text{I}\right)^2+\left(\text{tm6}-\frac{\text{D6}}{\text{vi}}-\mu\text{I}\right)^2+\left(\text{tm7}-\frac{\text{D7}}{\text{vi}}-\mu\text{I}\right)^2+\left(\text{tm8}-\frac{\text{D8}}{\text{vi}}-\mu\text{I}\right)^2+\left(\text{tm9}-\frac{\text{D9}}{\text{vi}}-\mu\right.$$

$$\left(\text{tm10}-\frac{\text{D10}}{\text{vi}}-\mu\text{I}\right)^2+\left(\text{tm11}-\frac{\text{D11}}{\text{vi}}-\mu\text{I}\right)^2+\left(\text{tm12}-\frac{\text{D12}}{\text{vi}}-\mu\text{I}\right)^2+\left(\text{tm13}-\frac{\text{D13}}{\text{vi}}-\mu\text{I}\right)^2+$$

$$\left(\text{tm14}-\frac{\text{D14}}{\text{vi}}-\mu\text{I}\right)^2+\left(\text{tm15}-\frac{\text{D15}}{\text{vi}}-\mu\text{I}\right)^2+\left(\text{tm16}-\frac{\text{D16}}{\text{vi}}-\mu\text{I}\right)^2+\left(\text{tm17}-\frac{\text{D17}}{\text{vi}}-\mu\text{I}\right)^2+$$

$$\left(\text{tm18}-\frac{\text{D18}}{\text{vi}}-\mu\text{I}\right)^2$$

$$\sigma\text{I}:=\sqrt{(\text{zI})/18}$$

$$\text{liI}:=\frac{(2\pi)^{-18/2}}{\sigma\text{I}^{18}}e^{-\text{zI}/2\sigma\text{I}^2}$$

BIC calculations

$$\text{BICI}=-2\text{Log}[\text{liI}]+\text{Log}[18]$$

9.21709

$$\text{BICTI}=-2\text{Log}[\text{liTI}]+3\text{Log}[18]$$

−59.5079